The Planetary Science Journal, 5:163 (29pp), 2024 July https://doi.org/10.3847/PSJ/ad3e80

Doomed Worlds. I. No New Evidence for Orbital Decay in a Long-term Survey of 43 Ultrahot Jupiters

Elisabeth R. Adams[1], Brian Jackson[2], Amanda A. Sickafoose[1], Jeffrey P. Morgenthaler[1], Hannah Worters[3], Hailey Stubbers[2], Dallon Carlson[2], Sakhee Bhure[4], Stijn Dekeyser[4], Chelsea X. Huang[4], and Nevin N. Weinberg[5]
[1] Planetary Science Institute, 1700 E. Ft. Lowell, Suite 106, Tucson, AZ 85719, USA; adams@psi.edu
[2] Department of Physics, Boise State University, 1910 University Drive, Boise, ID 83725-1570, USA
[3] South African Astronomical Observatory, 1 Observatory Road, Observatory, 7945, South Africa
[4] University of Southern Queensland, Centre for Astrophysics, West Street, Toowoomba, QLD 4350, Australia
[5] Department of Physics, University of Texas at Arlington, Arlington, TX 76019, USA
Received 2024 February 5; revised 2024 March 21; accepted 2024 March 23; published 2024 July 19

Abstract

Ultrahot Jupiters (UHJs) are likely doomed by tidal forces to undergo orbital decay and eventual disruption by their stars, but the timescale over which this process unfolds is unknown. We present results from a long-term project to monitor UHJ transits. We recovered WASP-12 b's orbital decay rate of $\dot{P} = -29.8 \pm 1.6$ ms yr^{-1}, in agreement with prior work. Five other systems initially had promising nonlinear transit ephemerides. However, a closer examination of two—WASP-19 b and CoRoT-2 b, both with prior tentative detections—revealed several independent errors with the literature timing data; after correction, neither planet shows signs of orbital decay. Meanwhile, a potential decreasing period for TrES-1 b, $\dot{P} = -16 \pm 5$ ms yr^{-1}, corresponds to a tidal quality factor $Q'_\star = 160$ and likely does not result from orbital decay if driven by dissipation within the host star. Nominal period increases in two systems, WASP-121 b and WASP-46 b, rest on a small handful of points. Only 1/43 planets (WASP-12 b) in our sample is experiencing detectable orbital decay. For nearly half (20/42), we can rule out $\dot{P}$ as high as observed for WASP-12 b. Thus, while many UHJs could still be experiencing rapid decay that we cannot yet detect, a sizable subpopulation of UHJs are decaying at least an order of magnitude more slowly than WASP-12 b. Our reanalysis of Kepler-1658 b with no new data finds that it remains a promising orbital decay candidate. Finally, we recommend that the scientific community take steps to avoid spurious detections through better management of the multi-decade-spanning data sets needed to search for and study planetary orbital decay.

Unified Astronomy Thesaurus concepts: Exoplanets (498); Hot Jupiters (753); Exoplanet tides (497); Transit timing variation method (1710); Transit photometry (1709)

Materials only available in the online version of record: machine-readable tables

1. Introduction

Ultrahot Jupiters (UHJs), or giant planets with orbital periods of less than about 3 days, experience significant tidal effects that play a critical role in their long-term dynamical stability. Recent work has shown that the population of all hot Jupiter ($P < 10$ days) host stars is younger than the general population of either field stars or planet-hosting stars (Hamer & Schlaufman 2019), and two separate analyses have found lower UHJ occurrence rates around older host stars (Chen et al. 2023; Miyazaki & Masuda 2023). All of this supports the idea that many giant, close-in planets quickly inspiral or are otherwise destroyed while their stars are still on the main sequence. Meanwhile, an estimated half of all stars may have ingested a former UHJ in the first <1 Gyr of the star's lifetime (Matsakos & Königl 2015). Recent direct detection of a planetary engulfment by De et al. (2023) for an inferred planet of 0.1–10 M_J came in the form of a low-luminosity optical transient lasting several days, followed by infrared brightening for several months. Such planet engulfment events are thought to occur somewhere in the galaxy about once every 1–10 yr (Metzger et al. 2012; De et al. 2023). Estimates for the lifetimes of UHJs as a population have been limited, however, by theoretical uncertainties in the value of the stellar tidal dissipation factor, $Q'_\star$, where estimates range from $10^{5.5}$–$10^{6.5}$ (Jackson et al. 2008; Husnoo et al. 2012) to $>10^7$–10^8 (Penev et al. 2012; Collier Cameron & Jardine 2018). More recent theoretical work that incorporates nonlinear dissipation has found important variations in $Q'_\star$ with stellar mass and age and that planets around stars with $M_\star \geqslant 1.2\ M_\odot$ only experience significant tidal decay when the star is on the subgiant branch (Weinberg et al. 2024). Penev et al. (2018) found a steep dependence on forcing frequency for $Q'_\star$, with $\log_{10} Q'_\star \sim 5$ for orbital periods $P \approx 2$ days increasing rapidly to $\log_{10} Q'_\star \sim 7.5$ for $P \approx 0.5$ day. Consequently, tidal decay might be expected to slow as the planet nears its star. It is important to note, however, that for planets whose rotation states are not tidally locked or whose orbits are eccentric, tidal decay can be driven by dissipation within the planet. However, tidal locking (Guillot & Showman 2002) and orbital circularization (Dawson & Johnson 2018) timescales for hot Jupiters are thought to be less than millions of years. Thus, in the absence of an exotic rotation state (Millholland & Laughlin 2018; Efroimsky & Makarov 2022) or dynamical excitation of eccentricity (Pu & Lai 2019), the contribution to tidal decay from dissipation within the planets is likely to be short-lived.

With a known population of around 100 UHJs, it is now possible to empirically address the open questions of how

many UHJs are in decaying orbits and at what rates they are decaying. Strong evidence for decay has been presented for just two UHJs, WASP-12 b (Patra et al. 2017; Baluev et al. 2019; Yee et al. 2020) and Kepler-1658 b (Vissapragada et al. 2022), with orbital periods that are apparently decreasing by -29 ± 2 ms yr^{-1} and -131 ± 22 ms yr^{-1}, respectively, corresponding to remaining lifetimes of 3 and 2.5 Myr. These decay rates also correspond to stellar tidal dissipation parameters of $Q'_\star = 1.8 \times 10^5$ and 2.5×10^4, respectively. Kepler-1658 b orbits an evolved subgiant ($M_\star = 1.45\ M_\odot$, $R_\star = 2.89\ R_\odot$) for which that rapid rate of decay matches the theoretical predictions of Vissapragada et al. (2022), though perhaps not those of Barker et al. (2024; see discussion in Section 6.7). Few planets are known around recently evolved stars due to challenges with their detection (see, e.g., Johnson et al. 2007). In fact, one explanation for the evolution of WASP-12 b may be that its host star is also a subgiant (Weinberg et al. 2017), though modeling and observational uncertainties leave its status ambiguous (Leonardi et al. 2024). This raises an open question: are there any UHJs around main-sequence stars with decaying orbits?

In the past few years, as observational baselines have passed the decade mark for many systems, a growing number of UHJs around main-sequence stars have been presented with suggestions that they may have decreasing orbital periods. These include HAT-P-19 b (Hagey et al. 2022); HAT-P-32 b (Hagey et al. 2022); HAT-P-51 b (Yeh et al. 2024); HAT-P-53 b (Yeh et al. 2024); KELT-9 b (Harre et al. 2023); TrES-1 b (Hagey et al. 2022; Ivshina & Winn 2022); TrES-2 b (Hagey et al. 2022); TrES-3 b (but noted to be marginal; Hagey et al. 2022; Mannaday et al. 2022); TrES-5 b (nonlinearity though not decay noted by Maciejewski et al. 2021; Hagey et al. 2022; Ivshina & Winn 2022; Yeh et al. 2024); WASP-4 b (Bouma et al. 2020; Hagey et al. 2022; Harre et al. 2023); WASP-19 b (Patra et al. 2020; Ivshina & Winn 2022); WASP-32 b (but not significant; Sun et al. 2023); WASP-43 b as reported by Sun et al. (2018), though not by Hagey et al. (2022); and XO-3 b (Ivshina & Winn 2022; Yang & Wei 2022). Many of these claimed detections are acknowledged in the original publications to be of marginal significance, however. It is also common for an apparent nonlinear ephemeris based on a small number of transits and/or a short baseline to disappear with additional observation (e.g., as for OGLE-TR-113 b; Adams et al. 2010; Hoyer et al. 2016). Even after an ostensible period decay is detected, it is necessary to rule out other physical mechanisms, such as apsidal precession (the current best explanation for KELT-9 b; Harre et al. 2023), perturbations caused by companion planets or stars, or even the acceleration of the host star toward the Earth (proposed as the explanation for WASP-4 b; Bouma et al. 2020).

Detecting orbital decay rewards a patient approach. Recent theoretical work by Jackson et al. (2023) has explored how repeated, regular observations of transits over a long timescale will detect planets with relatively fast, WASP-12 b–like rates of orbital decay, requiring roughly two transits per year for 10+ yr to build up clear evidence. Building on previous suggestions (Liddle 2007), that work focused on the Bayesian information criterion, or BIC (Schwarz 1978), both to judge whether a data set supports tidal decay and to design an observing program to optimally detect said decay. In this context, the BIC value can be defined as

$$\mathrm{BIC} = \chi^2 + k \ln N, \tag{1}$$

where N is the total number of data points, k is the number of fit parameters (two for a linear fit and three for a quadratic fit), and χ^2 measures the goodness of fit. The BIC value thus favors models that minimize residuals while penalizing additional model parameters. In the analysis that follows, we use two models: one with a linear term in orbital epoch (a linear ephemeris) and one with a quadratic term in orbital epoch (a quadratic ephemeris). The equation for a linear ephemeris is

$$T(E) = T_{0,\mathrm{lin}} + P_{\mathrm{lin}} \times E, \tag{2}$$

where the transit midtime, T, at a given epoch, E, may be predicted using the linear ephemeris reference time, $T_{0,\mathrm{lin}}$, at $E = 0$ and the orbital period, P_{lin}. The equation for a quadratic ephemeris is

$$T(E) = T_{0,\mathrm{quad}} + P_{\mathrm{quad}} \times E + \frac{1}{2}\frac{dP}{dE}E^2, \tag{3}$$

where dP/dE is the rate of change of the orbital period, P_{quad}, and $T_{0,\mathrm{quad}}$ is the quadratic ephemeris reference time.

Note that while the parameter used in the fit is typically dP/dE (which has units of days per epoch), the value most frequently quoted in the literature is the rate of change in ms yr^{-1}, or

$$\dot{P} = \left(\frac{dP}{dE}\right)[\mathrm{days\ epoch}^{-1}]\left(\frac{365.25}{P}\right)[\mathrm{epoch\ yr}^{-1}] \times (86{,}400)[\mathrm{s\ day}^{-1}](1000)[\mathrm{ms\ s}^{-1}], \tag{4}$$

where P is the orbital period in days, dP/dE is in days per epoch, and $\dot{P}$ is the rate of change of P in ms yr^{-1}.

To judge whether a linear or a quadratic ephemeris is favored by the data, we use the difference in the BIC values between the linear model ($\mathrm{BIC_{lin}}$) and the quadratic model ($\mathrm{BIC_{quad}}$):

$$\Delta\mathrm{BIC} = \mathrm{BIC_{lin}} - \mathrm{BIC_{quad}}. \tag{5}$$

A positive value of ΔBIC means that a quadratic ephemeris is preferred, and the higher the ΔBIC value, the higher the probability that the quadratic model (indicating possible orbital decay) is supported by the data over the linear (no tidal decay) model.

In this work, we present the first results of a new, long-term program to take regular ground-based observations of UHJs and combine these data with times from the literature, which for some planets stretch back over two decades. We have observed more than 100 new light curves of 43 UHJs for this project since 2022, and we are also publishing a cache of older light curves from 2008–2009 that had previously eluded publication. For this first paper, we summarize the results for all 43 systems but leave an in-depth analysis of most systems for future work. We focus here on six planets—CoRoT-2 b, TrES-1 b, WASP-12 b, WASP-19 b, WASP-46 b, and WASP-121 b—all of which initially had values for $\Delta\mathrm{BIC} \geqslant 30$ from calculations using our new midtimes and the midtimes recorded in the literature.

It is important to state from the outset that for two of the six planets we chose to focus on in this work—CoRoT-2 b and WASP-19 b, which initially had the largest ΔBIC values after WASP-12 b—we needed to correct numerous errors and inconsistencies in the literature. After doing so, our final ΔBIC values for both planets dropped so significantly that neither one of them now shows any signs of nonlinear ephemerides. WASP-12 b remains the *only* candidate in our sample with evidence for orbital decay. (Notably, our sample does not

include Kepler-1658 b, for which we have no new observations: its depth of 0.1% makes it difficult to observe except from space or from the largest ground-based observatories. We do, however, apply the same analysis to the existing data for Kepler-1658 b and find it to be a very promising candidate, as discussed in Section 6.7.)

In Section 2, we discuss the new ground-based observations and describe the photometry methods used to create the new transit light curves. Data from TESS and CoRoT are described in Section 3. We describe our transit light-curve fitting method in Section 4. In Section 5, we describe challenges in compiling the literature data and detail several issues that we uncovered with published transit midtime values. In Section 6, we describe our best current analysis of the timing for each of the six planets we are exploring in detail, plus Kepler-1658 b. In Section 7, we discuss what the results mean for the population of UHJs and the values of $Q'_\star$ for their host stars. As discussed above, tidal dissipation within the planet could contribute to decay, but we have no evidence either that the planets we study here are not tidally locked or have eccentric orbits, so we neglect this contribution. Consequently, the constraints we report on $Q'_\star$ represent lower limits. We conclude in Section 8 with some recommendations for best practices for searches for orbital decay and a proposal for better management of transit timing data to prevent unnecessary errors in the future, which will enable the detection of subtle timing effects that unfold over many years across large, inhomogeneous data sets.

2. New Ground-based Observations and Photometry

In this paper, we are publishing the photometry for 23 new transits of six planets: CoRoT-2 b, TrES-1 b, WASP-12 b, WASP-19 b, WASP-46 b, and WASP-121 b, shown in Figure 1. (To allow for more in-depth analyses of individual systems, transit light-curve photometry and full timing analyses for the other 37 planets in our sample will be published in future works. The results presented in this work for those 37 systems are based on at least one new light curve along with the literature transit midtimes compiled as in Section 5, although no attempt has been made to correct literature times except for removing obvious duplicates.) Five ground-based observatories produced these observations in 2008–2009 and 2022–2023, with observational details shown in Table 1. All ground-based, TESS, and CoRoT light curves for the six planets featured in this work are available as supplementary data, with a stub table for format in Table 2.

2.1. Io Input/Output Observatory Observations

The Planetary Science Institute's Io Input/Output Observatory (IoIO) is a small-aperture (35 cm) robotic telescope located at the San Pedro Valley Observatory, a hosting site situated in a dark location 100 km east of Tucson, Arizona. IoIO was purpose-built to record observations of faint gases around Jupiter that trace their origin from Jupiter's moon Io and as such has a built-in coronagraph (for more details about the observatory, see, e.g., Morgenthaler et al. 2019), but it is also a fully functional general-purpose telescope. Since 2022, much of the time when Jupiter is not available has been dedicated to exoplanet transits, and we have successfully observed over 100 full or partial exoplanet transits, six of whose light curves are published in this work. Observations in 2022–2023 were scripted to be taken in the *R* filter at an exposure time chosen for the magnitude of the host star. For two transits of WASP-12 b, bad weather or scheduling issues resulted in only partial observations over egress.

The timescale for all IoIO observations is determined using the system clock of the observatory control computer, which is maintained to within ∼3 ms rms of UTC using the Network Time Protocol system. However, variable latencies in the Windows 10 operating system, the USB 2.0 link between the computer and Starlight Xpress SX694, and the camera itself contribute to a 0.230 s uncertainty in the observation midpoints for exposures of >0.7 s (all of the IoIO data presented here) and 0.160 s for exposures of <=0.7 s. This discontinuity has its roots in a decision the MaxIm DL Pro Starlight XPress camera plug-in makes about where the exposure time clock is maintained: in the camera (exposures of <=0.7 s) or within the MaxIm DL software (exposures of >0.7 s). This discontinuity, and thousands of photometric observations of stars recorded since 2019, has made derivation of the quoted uncertainties possible.

Light curves for data taken with IoIO are created through the automatic processing scripts. Photometry is accomplished by creating a segmentation image using photutils (Bradley et al. 2019). This approach, more widely used among extragalactic astronomers for isolating galaxies in crowded fields, has the advantage that it is largely agnostic to issues that distort stellar images. For the IoIO coronagraph, these issues include a variable point-spread function (PSF) across the field of view and wind shake. Standard CCD processing steps, such as bias subtraction, masking of hot pixels, and flat-fielding, are conducted using a customization of several astropy tools in a multiprocessing, pipeline-oriented code (Craig et al. 2017; Astropy Collaboration et al. 2022; Morgenthaler 2022, 2023a, 2023b). Then, each image is convolved by a 3 pixel FWHM 2D Gaussian kernel to enhance stellar sources. A preliminary source mask is created to enable optimal background estimation. The critical step in creating the segmentation image is to set the threshold above the local background level that triggers identification of a source. We use 5 times the rms variation in the background. The segmentation image is created assuming that a minimum-sized source is formed by 5 connected pixels. Blended sources within the image are separated using a combination of multithresholding and watershed segmentation, as per the photutils algorithm, with the number of multithresholding levels set to 32 and contrast = 0.001. This procedure results in well-identified sources in most cases, even if the stellar images are not round. The segmentation image is transformed into a mask that is applied to the original image and used together with the calculated background image to extract source parameters, such as centroid and flux. Astrometry on the source centroids is performed using the astrometry.net software (Lang et al. 2010), and the resulting source table is recorded in an Astropy Enhanced Character-Separated Variable file. We then performed differential photometry using the star counts for the target star and at least one other nearby companion star, as described in Section 2.3.

2.2. South African Astronomical Observatory 40 inch Observations

Observations were taken on the 40 inch telescope operated by the South African Astronomical Observatory (SAAO) in Sutherland, South Africa, using the Sutherland High-speed Optical Camera facility instruments (Coppejans et al. 2013).

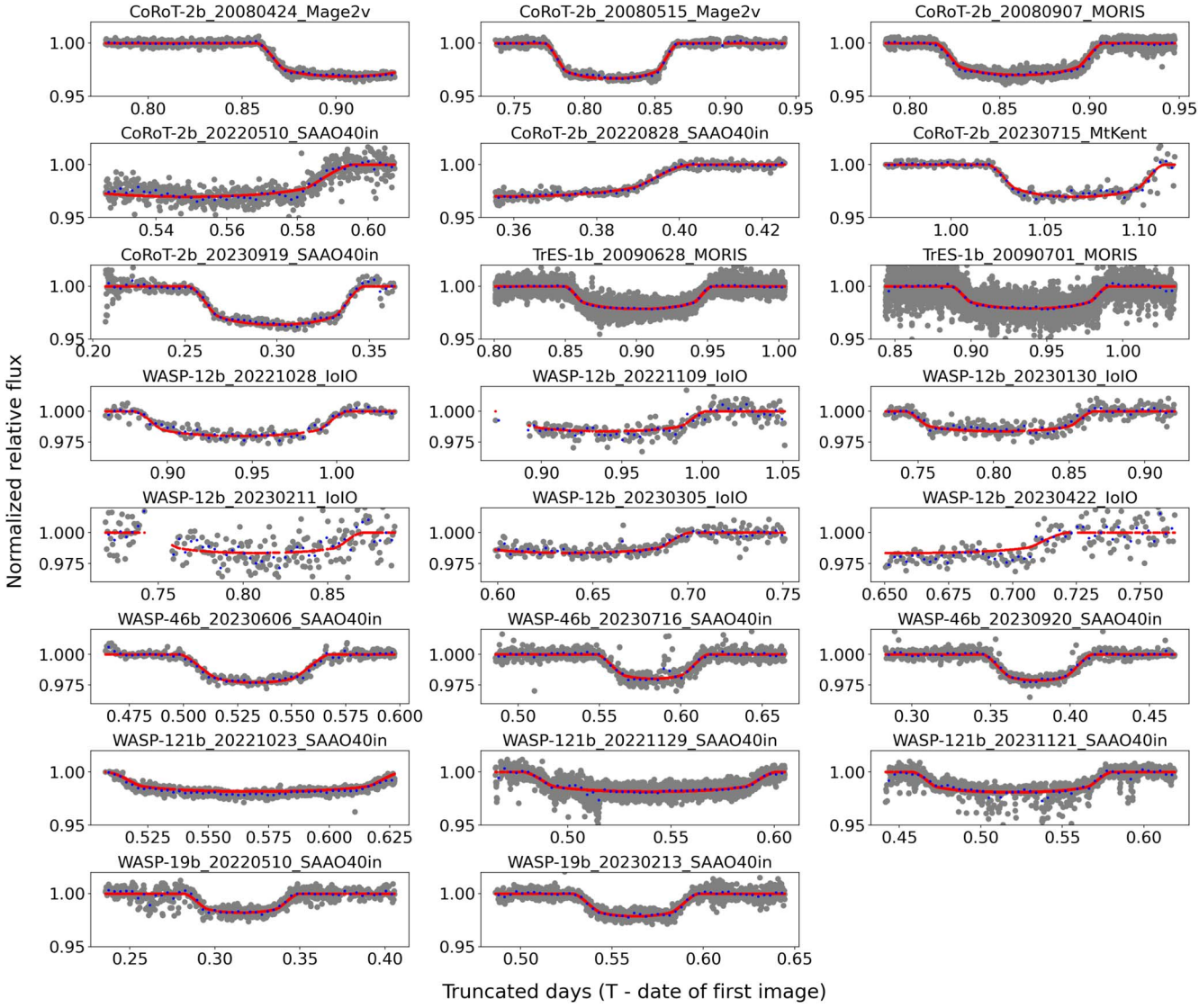

Figure 1. Twenty-three new light curves of six planets: CoRoT-2 b, TrES-1 b, WASP-12 b, WASP-19 b, WASP-46 b, and WASP-121 b. The date and site of each observation are given in the panel header (see Section 2). Normalized relative flux is plotted vs. truncated time, where the time of the first observation in each sequence has been subtracted for clarity of display. Data are shown as gray points, with binned data shown as blue points. A transit light-curve model fit is overplotted in red. These light curves are available as supplementary data.

These instruments are ideal for exoplanet observations, as they were built to be optimized for high-speed, accurately timed imaging. They employ Andor iXon 888 frame-transfer EMCCD cameras that are triggered by GPS, mounted with a suite of Johnson–Cousins and Sloan filters and an open-filter setting. Observations were mostly taken in *R*, with other details in Table 1. All data were taken with 2×2 binning ($0\farcs334$ superpixel^{-1}), the 3 MHz conventional mode, and the $5.2\times$ gain setting (8.6 electrons ADU^{-1}). Biases and twilight flats were taken each night of the observations, and all data were bias-subtracted and flat-fielded. For two transits of CoRoT-2 b and one transit of WASP-12 b, bad weather and/or scheduling issues resulted in only partial observations over ingress and/or egress.

The SAAO 40 inch images have a modest $2\farcm85 \times 2\farcm85$ field of view that typically contains a handful of well-separated companion stars. Target star counts were calculated using the astropy affiliate package photutils (Bradley et al. 2019) for the target and at least one nearby companion star using circular apertures in a range of sizes (eight apertures between 8 and 25 pixels) to provide stellar locations and counts. None of the six targets in this paper are in crowded enough fields to require PSF photometry. We performed differential photometry using the star counts for the target star and at least one other nearby companion star, as described in Section 2.3.

2.3. Differential Photometry of IoIO and SAAO 40 inch Data

We fed the lists of star counts (produced as described above) into a common python-based pipeline to find the aperture and combination of comparison stars that produced the best light curve (nominally, the one with the lowest scatter on the out-of-transit baseline). While differential aperture photometry is simple in concept, in practice, it is complicated to construct a robust automated pipeline that can efficiently process ground-based data from multiple instruments and spanning a wide range of target star magnitudes, available comparison stars (from empty fields with one very faint comparison star to crowded fields with 100+ stars to choose between), different

Table 1
Observational Details

Planet	Date[a]	Instr.	Time (hr)	$N_{\rm frames}$ (use)	$N_{\rm frames}$ (omit)	$N_{\rm c}$[b]	Filter	Exp. (s)	Aper. (pixels)	Scatter[c] (%)
CoRoT-2 b	2008 Apr 24	Mage2v	3.7	1156	0	1	*i*	5–10	18	0.19
CoRoT-2 b	2008 May 15	Mage2v	4.9	1214	0	1	*i*	4–10	16	0.2
CoRoT-2 b	2008 Sep 7	MORIS	3.9	2707	0	1	*R*	5	26	0.32
CoRoT-2 b	2022 May 11	SAAO40in	2.0	755	0	4	*R*	8–10	18	0.74
CoRoT-2 b	2022 Aug 28	SAAO40in	2.3	410	40	1	*R*	5–25	18	0.27
CoRoT-2 b	2023 Jul 15	MINERVA	3.7	203	0	2	Clear	60	21	0.47
CoRoT-2 b	2023 Sep 19	SAAO40in	3.8	357	0	1	*R*	8–60	8	0.55
TrES-1 b	2009 Jun 28	MORIS	4.9	9993	0	1	*R*	1	32	0.43
TrES-1 b	2009 Jul 1	MORIS	4.6	7994	0	1	*R*	2	36	0.82
WASP-12 b	2022 Oct 28	IoIO	4.3	179	3	8	*R*	42.71	NA[d]	0.32
WASP-12 b	2022 Nov 9	IoIO	4.4	276	5	1	*R*	42.71	NA[d]	0.55
WASP-12 b	2023 Jan 30	IoIO	4.9	329	0	12	*R*	42.71	NA[d]	0.4
WASP-12 b	2023 Feb 11	IoIO	4.1	221	28	1	*R*	42.71	NA[d]	1.11
WASP-12 b	2023 Mar 5	IoIO	3.6	237	2	8	*R*	42.71	NA[d]	0.41
WASP-12 b	2023 Apr 22	IoIO	3.6	202	14	16	*R*	42.71	NA[d]	0.82
WASP-46 b	2023 Jun 6	SAAO40in	3.2	357	0	1	*R*	20–45	8	0.26
WASP-46 b	2023 Jul 16	SAAO40in	4.3	761	0	1	*R*	15–35	8	0.43
WASP-46 b	2023 Sep 20	SAAO40in	4.4	615	0	1	*R*	20–35	12	0.32
WASP-121 b	2022 Oct 24	SAAO40in	2.9	1133	1	3	*R*	8–10	25	0.24
WASP-121 b	2022 Nov 29	SAAO40in	5.0	4062	210	1	*R*	3–6	15	0.48
WASP-121 b	2023 Nov 21	SAAO40in	4.3	1297	135	3	*R*	10–15	18	0.58
WASP-19 b	2022 May 10	SAAO40in	4.1	756	74	1	*R*	15–25	12	0.47
WASP-19 b	2023 Feb 13	SAAO40in	3.8	1316	10	3	*R*	8–15	10	0.4

Notes.
[a] Date of first observation in time series; may differ from transit name in Figure 1 assigned by observing night.
[b] Number of comparison stars used in light curve.
[c] Standard deviation of residuals (normalized flux minus model).
[d] Aperture photometry not used; see discussion in Section 2.1.

aperture sizes, instrumentation quirks (e.g., target drift, wind shake, or telescope pointing jumps), and variable weather conditions.

The pipeline tracks stars through pointing jumps or slow drifts, and it can be run iteratively to explore the effects of removing one or more comparison stars and/or image frames. Images are removed if they are missing the target star and/or one or more critical comparison stars, or if the stars are streaked due to telescope motion. Importantly, the light-curve generation notebooks and scripts are quasi-automated, meaning that light curves can be automatically run with default settings appropriate to the selected instrument and planet, but each transit light curve may also be manually adjusted to account for conditions unique to that transit.

For each target star, the pipeline specifies a default range of star brightnesses relative to the target for acceptable comparison stars. It then calculates the ratio of the target star to each potential companion star and rejects those with scatter above a particular threshold (adjustable for each target star). Comparison stars that were not present on every field (typically due to tracking motion or variable cloud conditions causing stars to either saturate or become too faint) are automatically removed. Other problematic stars, e.g., strongly variable stars, can be excluded for individual transits as needed. There is also a mechanism to identify bad frames in cases where all comparison stars are lost; after omitting those frames, comparison star selection proceeds as above using the remaining good frames. Table 1 shows the number of frames and comparison stars used for each light curve. Once the best set of comparison stars has been identified, a normalized transit light curve is produced for each aperture: the counts from the target star are divided by the sum of the counts of the companion stars, then normalized by dividing by the median flux outside of the predicted transit window. The best aperture is the one that minimizes the scatter on the out-of-transit baseline (see Table 1). Sometimes the resulting transit has a slope in the overall flux, often correlated with the air mass of the target star. We leave detrending any such slopes as a free parameter during fitting (Section 4).

2.4. MINERVA-Australis Observations and Photometry

One transit of CoRoT-2 b was observed with the MINERVA-Australis telescope array (Addison et al. 2019), located at Mt. Kent Observatory, Australia. MINERVA-Australis is an array of four identical 0.7 m telescopes linked via fiber feeds to a single high-resolution spectrograph. The array has been wholly dedicated to radial velocity follow-up of TESS planet candidates (e.g., Nielsen et al. 2019; Addison et al. 2021; Wittenmyer et al. 2022). Each telescope is now able to operate in photometric mode using a flip mirror that redirects light to cameras located at the Nasmyth focus. The observations described here were obtained with a ZWO1600 CMOS camera using 4×4 binning, with the images slightly defocused (the PSF FWHM was 5.05 pixels or $3\farcs41$). The MINERVA telescopes log GPS-based time stamps that are then converted to Barycentric Julian Date (BJD) time stamps using the JDUTC to BDJTDB time converter that is part of the barycorrpy package (Kanodia & Wright 2018).

An instrumental glitch in the middle of the sequence caused a jump with image rotation, followed by slow derotation back

Table 2
Transit Light Curves Used in Fits in This Work for Six Planets[a]

Transit	Planet	Instrument[b]	Time (BJD/TDB)[c]	Flux[d]	Model[e]
CoRoT-2b_20080424_Mage2v	CoRoT-2 b	Mage2v	2454580.7772671296	0.999115	1.0
CoRoT-2b_20080424_Mage2v	CoRoT-2 b	Mage2v	2454580.7774444446	1.002975	1.0
CoRoT-2b_20080424_Mage2v	CoRoT-2 b	Mage2v	2454580.777630324	1.00391	1.0
CoRoT-2b_20080424_Mage2v	CoRoT-2 b	Mage2v	2454580.777815162	1.001988	1.0
CoRoT-2b_20080424_Mage2v	CoRoT-2 b	Mage2v	2454580.7780003473	0.998502	1.0

Notes.
[a] CoRoT-2 b, TrES-1 b, WASP-12 b, WASP-19 b, WASP-46 b, and WASP-121 b.
[b] Ground-based: 23 transits (see Figure 1). CoRoT: 82 transits. TESS: 333 transits.
[c] Time at midexposure. Time system used is BJD in TDB.
[d] Normalized detrended flux of planet-hosting star.
[e] Model flux for each time in the light curve, using the best-fit models for each transit as described in Section 4.
(This table is available in its entirety in machine-readable form in the online article.)

to the original alignment, which, combined with deteriorating weather, resulted in poorer data quality after midtransit. To control for the effect of the rotation, the final light curve was created using a separate Mathematica photometry notebook to do differential circular-aperture photometry on the target star and two nearby, bright comparisons. Stars were centroided on every frame to determine the centers of the apertures. For each star, three hand-selected boxes well outside of the apertures and without stars were used to determine the background value. The final light curve was generated by subtracting the background counts from each star, dividing the target by the average signal of the comparison stars, and normalizing to the median out-of-transit baseline. The lowest baseline scatter was achieved with an aperture 21 pixels in diameter.

2.5. Infrared Telescope Facility and Las Campanas Observatory Observations and Photometry

Three transits of CoRoT-2 b were observed in 2008 shortly after the planet's discovery was announced, and they were included in Adams (2010), but the light curves have not been published until now. Two transits were taken on the 6.5 m Magellan Clay telescope at Las Campanas Observatory (LCO) on 2008 April 24 and 2008 May 15 during the first observing runs to use the updated MagIC-e2v camera (see, e.g., Osip et al. 2004; Adams et al. 2011). MagIC-e2v had 1024×1024 pixels, each 13 μm square, and on Magellan had a field of view of $38'' \times 38''$ and a plate scale of $0\farcs037\,\mathrm{pixel}^{-1}$ unbinned. The timing for these observations came from network computers that were verified each evening to be synced within a second to UTC standard. Note that the partial transit on 2008 April 24 was deliberately scheduled right before dawn after two other transits were observed that night and is not due to weather.

The third transit of CoRoT-2 b on 2008 September 7 was observed using the MIT Optical Rapid Imaging System (MORIS) on NASA's 3 m Infrared Telescope Facility (IRTF; Gulbis et al. 2011). A dichroic was used to direct light <0.95 μm to MORIS through a Thor long-pass red visitor filter with a lower cutoff at 700 nm. The plate scale for MORIS is $0\farcs114\,\mathrm{pixel}^{-1}$, with a $60'' \times 60''$ field of view. We used the 1 MHz conventional mode in a 2.4× gain setting, which has a read noise of $6\,e^-\,\mathrm{pixel}^{-1}$ and gain of $1.5\,e^-\,\mathrm{ADU}^{-1}$. MORIS observations were triggered by GPS and had better than microsecond timing accuracy.

Additionally, we observed two transits of TrES-1 b using MORIS on the IRTF on 2009 June 28 and 2009 July 1 using the same settings as for CoRoT-2 b, which have not been previously published. Observational details for all of the IRTF and LCO transits are included in Table 1.

All of the data from 2008 to 2009 were reduced using a Mathematica-based differential aperture photometry pipeline described in Adams (2010). We have elected to keep the original photometry, but we have fit new transit light-curve models using the fitting method described in Section 4.

3. Data from Space Telescopes

In addition to new ground-based observations, we present new fit results to light curves from at least one TESS sector for all six planets and new fits for the CoRoT mission data for CoRoT-2 b. Although all space-based data used to make these light curves are publicly available and should remain that way in perpetuity, the version of the data available to the public may change in the future (as happened for the CoRoT data). The TESS data also required nontrivial processing (smoothing and detrending) to produce these light curves. For these reasons, we consider it important to publish the version of the transit light curves that we fit in this work, so as to make it as easy as possible to reproduce our results and/or to identify the source of problems that may come to light in the future. All transit light curves may be found in a supplementary electronic file, with a stub table for format at Table 2.

3.1. TESS Photometry

Where available, we used the published transit midtimes for TESS transits found in Ivshina & Winn (2022). That work required that transits have at least 75% of the expected number of data points per transit interval, and we have added midtimes for some partial light curves that were omitted from earlier sectors, as well as sectors that have been released since it was published. We fit a total of 193 TESS light curves to each of six planets as follows: CoRoT-2 b (Sector 54: 12, total: 12); TrES-1 b (Sector 14: 2, Sector 40: 1, Sector 53: 7, Sector 54: 8, total: 18); WASP-12 b (Sector 43: 3, Sector 44: 20, Sector 45: 21, total: 44); WASP-19 b (Sector 09: 2, Sector 36: 5, Sector 62: 32, Sector 63: 33, total: 72); WASP-46 b (Sector 01: 3, Sector 27: 2, Sector 67: 20, total: 22); and WASP-121 b (Sector 07: 1, Sector 34: 1, Sector 61: 20, total: 22).

We used the python package lightkurve to download and analyze the 120 s cadence data (MAST Team 2021). To condition the TESS data, we first masked out sections

containing bad data. Because TESS light curves span the full transit orbital period, they often exhibit more long-term stellar variability than do ground-based data, which only last a few hours. We found detrending for long-period variability to be necessary before fitting. We masked out the time during planetary transit to interpolate a smoothing function for each sector using a smoothing window between 21 and 501 frames, depending on the cadence and the target, with the built-in "flatten" method in lightkurve. We then divided the full time series by the smoothed light curve and normalized the light curve. We divided each sector into chunks centered on each transit; all of the transits in this paper had sufficient signal-to-noise to be independently fit to a transit light-curve model.

3.2. CoRoT Photometry

For CoRoT-2 b, we downloaded data from the LEGACY data release (version 4).[6] We used the red flux (keyword "REDFLUX"), which was less noisy than either the green or the blue fluxes, and the frame times given in BJD/TT (keyword "DATEBARTT"); for an explanation of why the ms-level difference between Terrestrial Time (TT) and Barycentric Dynamical Time (TDB) is not important for our purposes, see the discussion of timing systems in Section 5.3. For CoRoT-2 b, the first three transits (out of 82) in the 150 day sequence were recorded at the longer cadence (512 s), at which point the transit signature was identified by the CoRoT team, and the rest of the data were taken at 32 s. We chose not to smooth and flatten the CoRoT data in the same way as we did the TESS data but instead use a subset of the data in an 8 hr window centered around the predicted transit midtime. The linear term in our fit function accounted for any remaining trends, which were slight.

4. Transit Light-curve Fitting

Each transit light curve was fit using Markov Chain Monte Carlo methods using the publicly available python package PyLightcurve (Tsiaras et al. 2016), which is based on Emcee, an affine-invariant ensemble sampler (Foreman-Mackey et al. 2013), and makes use of several other scientific packages and catalogs.[7] For each fit, we used 400 walkers and 150,000 links, with the first 30,000 links as burn-in. Convergence of chains was checked by examining the autocorrelation time as well as the traces and the correlations between parameters for signs of nonconvergence.

Our focus for this work is on the timing, and most of the transit light-curve parameters were fixed to the best-fit parameters from more precise light curves, including the eccentricity (e), the inclination (i), and the ratio of the orbital semimajor axis to the stellar radius $a/R_\star$. We used the values reported in Table 3 taken from the Exoplanet Characterization Catalog, which was developed for the ExoClock project (Kokori et al. 2022), with missing or (rarely) inaccurate parameters replaced by values from the the NASA Exoplanet Archive where necessary. Note that for most light curves in this work, the signal-to-noise ratio is modest enough that the fitted transit midtime values are quite insensitive to the choice of values for, e.g., $a/R_\star$ or the limb-darkening coefficients. We nonetheless verified that the fits were reasonable by checking for abnormal scatter in the residuals from the model fits, especially around ingress and egress where issues with the shape are most evident. Limb-darkening coefficients were calculated for the appropriate bandpass in pylightcuve using ExoTethys (Morello et al. 2020a). For the six planets that are the focus of this work—CoRoT-2 b, TrES-1 b, WASP-12 b, WASP-19 b, WASP-46 b, and WASP-121 b—we have published all parameters, fitted and fixed, for each light curve that we fit, including those from CoRoT and TESS, which are available as a supplementary table with a stub table for format at Table 4. We are also publishing the transit midtimes and errors as a stand-alone table, along with their timing systems and sources, to aid future timing analysis efforts (Table 5).

We fit each light curve individually with a default of four free parameters—$T_{\rm mid}$, $r_p/R_\star$, N, and L—where r_p is the planetary radius, $R_\star$ is the stellar radius, N is the normalization constant (typically very close to 1), and L is a linear term to account for any residual slopes in the light curve. Some transits with a photometric discontinuity were fit jointly as two partial transits with the same radius ratio and midtime but separate N and L values. For partial transits, we did not fit for L. We examined fitting all light curves for a given planet together jointly; however, given the number of fixed parameters, joint fitting would only be helpful for multiple light curves observed with the same filter, which would be expected to share a common value for $r_p/R_\star$. In practice, joint fits were time-consuming to rerun each time new observations were added and did not yield significantly different results, so we have used individual transit fits in this work.

5. Curation of Literature Light-curve Times

Although regular new observations are key to a long-term project such as this one, it is the entire cumulative body of transit knowledge that allows us to make sensitive timing measurements. For several targets, the literature data now span two decades, and some planets have 10+ reference works containing hundreds of transits observed on many telescopes using a variety of methods to generate and fit the transit light curves. Since most of these works contain a mix of new data, reanalyzed data, and times drawn directly or with some correction from the literature, data curation has become and will remain a large component of precise timing analysis. We discuss below some of the lessons learned, including the importance of identifying duplicated times (Section 5.1) and composite times (Section 5.2) and the ever-present pitfall of improper conversion between the JD/UTC and BJD/TDB timing systems (Section 5.3).

As our starting point for compiling the literature midtimes, we used the work of Ivshina & Winn (2022), which contains both new analyses of TESS light curves and a thorough literature review through 2022 for hundreds of hot Jupiters. Although we have identified some errors in Ivshina & Winn (2022) that are discussed below, as is perhaps inevitable for any static database of this magnitude, we note that their work represents a formidable contribution to the timing literature. In particular, the table in Ivshina & Winn (2022) has two extremely useful features for error corrections: (1) it converts the literature times into the BJD/TDB time system wherever possible and explicitly states the time system used, and (2) it provides the Astrophysics Data System code for the paper where each transit midtime was reported, making it easier to identify the source of every reported

[6] http://idoc-corot.ias.u-psud.fr/sitools/client-user/COROT_N2_PUBLIC_DATA/project-index.html

[7] matplotlib (Hunter 2007); ExoTETHyS (Morello et al. 2020b); Exoplanet Characterization Catalog (Kokori et al. 2022); astropy (Astropy Collaboration et al. 2013); SciPy (Virtanen et al. 2020); NumPy (Oliphant 2006).

Table 3
Stellar and Planetary Parameters and Summary of Transits Available for 43 Planets

Planet	Value Used[a]							Observations		
	P (days)	$a/R_\star$	i	M_p	$M_\star$	$R_\star$	Age (Gyr)	N_{tr}[b]	Epochs[c]	Years[d]
CoRoT-2 b	1.743	6.7	87.8	3.47	0.96	0.96	0.3	164	3810	18
HAT-P-23 b	1.21289	4.55	85.7	2.09	1.13	1.13	4.0(1.0)	125	4603	15
HAT-P-36 b	1.32735	4.67	85.2	1.85	1.03	1.03	$6.6^{+2.9}_{-1.8}$	129	3421	12
HATS-24 b	1.3485	4.67	86.6	2.26	1.07	1.07	$3.7^{+2.0}_{-1.8}$	54	2301	8
HATS-35 b	1.821	4.79	86.9	1.22	1.32	1.32	2.13(0.51)	22	1573	8
HATS-70 b	1.88824	4.17	86.7	12.9	1.78	1.78	$0.81^{+0.50}_{-0.33}$	20	1798	9
HIP 65 A b	0.98097	5.29	77.2	3.21	0.78	0.78	$4.1^{+4.3}_{-2.8}$	106	1919	5
KELT-16 b	0.96899	3.23	84.4	2.75	1.21	1.21	3.1(0.3)	93	3032	8
KELT-1 b	1.21749	3.69	86.8	27.23	1.32	1.32	⋯	33	3288	11
KOI-13 b	1.76359	4.5	86.8	9.28	1.72	1.72	0.5(0.1)	8	2508	12
KPS-1 b	1.70633	6.37	83.2	1.09	0.89	0.89	⋯	54	1521	7
Qatar-10 b	1.64533	4.9	85.9	0.74	1.16	1.16	3.2(1.9)	217	1111	5
Qatar-1 b	1.42002	6.25	84.1	1.29	0.84	0.84	$11.6^{+0.60}_{-4.70}$	266	3241	13
Qatar-2 b	1.33712	6.45	89.0	2.49	0.74	0.74	1.4(0.3)	75	3354	12
TOI-2046 b	1.49719	4.75	83.6	2.3	1.13	1.13	$0.45^{+0.43}_{-0.021}$	102	883	4
TOI-2109 b	0.67247	2.27	70.7	5.02	1.45	1.45	1.77(0.88)	97	1723	3
TOI-564 b	1.65114	5.32	78.4	1.46	1.0	1.0	7.3	54	943	4
TrES-1 b	3.03007	10.52	90.0	0.84	1.04	1.04	$3.7^{+3.4}_{-2.8}$	129	2293	19
TrES-2 b	2.47061	7.9	83.9	1.49	1.36	1.36	$5.0^{+2.7}_{-2.1}$	228	2526	17
TrES-3 b	1.30619	6.0	82.0	1.91	0.93	0.93	$0.90^{+2.80}_{-0.80}$	387	4545	16
WASP-103 b	0.92555	3.01	88.2	1.49	1.22	1.22	4.0(1.0)	55	3959	10
WASP-104 b	1.75541	6.52	83.6	1.27	1.08	1.08	3	124	2098	10
WASP-114 b	1.54877	4.29	84.0	1.77	1.29	1.29	$4.3^{+1.4}_{-1.3}$	16	2218	9
WASP-121 b	1.27492	3.75	87.6	1.16	1.36	1.36	1.5(1.0)	93	2851	10
WASP-12 b	1.09142	3.04	83.4	1.47	1.43	1.43	2	223	5077	15
WASP-135 b	1.40138	5.53	82.0	1.9	0.98	0.98	0.6	54	3490	13
WASP-145A b	1.76904	8.09	83.3	0.89	0.76	0.76	6.99	21	1865	9
WASP-163 b	1.60969	5.62	85.4	1.87	0.97	0.97	⋯	15	1352	6
WASP-164 b	1.77714	6.5	82.7	2.13	0.95	0.95	4.08	20	1675	8
WASP-173A b	1.38665	4.78	85.2	3.69	1.05	1.05	6.78(2.93)	42	2150	8
WASP-18 b	0.94145	3.56	84.9	10.2	1.29	1.29	0.5	108	12,228	32
WASP-19 b	0.78884	3.46	78.8	1.15	0.96	0.96	$5.5^{+8.5}_{-4.5}$	244	6714	15
WASP-32 b	2.71866	7.8	85.3	2.63	0.72	0.72	2.22	22	1850	14
WASP-33 b	1.21987	3.79	87.7	2.09	1.5	1.5	⋯	102	4711	16
WASP-36 b	1.53737	5.85	83.2	2.36	1.08	1.08	2.5	93	2919	12
WASP-3 b	1.84684	5.0	84.2	2.43	1.62	1.62	2.1	142	3205	16
WASP-43 b	0.81347	4.87	82.1	1.78	0.58	0.58	7.0(7.0)	224	5589	12
WASP-46 b	1.43037	5.85	82.8	1.91	0.83	0.83	$9.6^{+3.7}_{-4.2}$	142	3364	13
WASP-50 b	1.95509	7.53	84.7	1.47	0.89	0.89	7	51	2177	12
WASP-52 b	1.74978	7.38	85.3	0.46	0.87	0.87	⋯	153	2565	12
WASP-5 b	1.62843	5.37	85.6	1.58	0.96	0.96	5.6	73	3851	17
WASP-64 b	1.57329	5.39	86.6	1.27	1.0	1.0	7	80	2993	13
WASP-77A b	1.36003	5.41	89.4	1.67	0.9	0.9	$6.2^{+4.0}_{-3.5}$	50	2898	11

Notes.
[a] From the Exoplanet Characterization Catalog (Kokori et al. 2022) and NASA Exoplanet Archive.
[b] Number of transit midtimes used in this work.
[c] Number of epochs between first and last transit midtime.
[d] Years spanned by observed transit midtimes.

midtime. Without these features it would have been much harder to uncover the errors that we have found.

Our second main source of transit midtimes is the Exoplanet Transit Database, or ETD,[8] which provides an online repository for light curves from amateur astronomers, who have posted tens of thousands of light curves of hundreds of systems since the website went online in 2008 September (Poddaný et al. 2010). Although the data on the ETD can vary widely in quality, many planets have been observed with nearly continuous timing coverage, a key feature for constraining long-term timing variations. For each planet, the ETD provides a table listing all of their available midtimes, which we used with three additional cuts to the data: (1) for systems with many transits, we selected the highest-quality data flag (DQ = 1 for CoRoT-2 b, TrES-1 b, WASP-12 b, and WASP-19 b and DQ = 1 or 2 for WASP-46 b and WASP-121 b); (2) we removed all transits with very large midtime errors

[8] http://var2.astro.cz/ETD/

Table 4
Fit Parameters for Transit Light Curves of Six Planets[a]

Parameter	Value	Err. Minus[b]	Err. Plus
Planet	CoRoT-2 b	⋯	⋯
Transit number	0	⋯	⋯
Transit name	CoRoT-2b_20070517-00_CoRoT	⋯	⋯
$T_{\rm mid}$ [BJD/TDB]	2454237.5345	0.0017	0.0013
$a/R_\star$	6.7	⋯	⋯
i (deg)	87.84	⋯	⋯
e	0.0	⋯	⋯
ω	0.0	⋯	⋯
ldc1[b]	0.5179	⋯	⋯
ldc2[b]	−0.1524	⋯	⋯
ldc3[b]	0.6843	⋯	⋯
ldc4[b]	−0.3178	⋯	⋯
N	0.9988	0.00034	0.00039
L	0.019	0.0019	0.0019

Notes.
[a] CoRoT-2 b, TrES-1 b, WASP-12 b, WASP-19 b, WASP-46 b, and WASP-121 b.
[b] Parameters with no errors were fixed in the fits.
[c] Limb-darkening coefficients from ExoTethys (Morello et al. 2020a).

(This table is available in its entirety in machine-readable form in the online article.)

(>5 minutes); and (3) we removed duplicate times that are in the ETD but are also in Ivshina & Winn (2022), preferring the values from Ivshina & Winn (2022), which are in the BJD/TDB system (the ETD uses HJD/UT; see discussion of timing systems in Section 5.3). Looking for duplicate transits had to be done by hand to ensure that we did not inadvertently remove points that were observed on the same night but at two different sites and will now be discussed in more detail.

5.1. Multiple Reported Transit Midtimes for the Same Epoch

When results are combined from many sources, it is common for there to be multiple, nonidentical transit midtimes reported at the same transit epoch. The challenge is to identify which are duplicates that need to be weeded out and which are simultaneous observations that should be kept. We have found at least four ways in which repeats occur: (1) two or more telescopes were used to observe during the same transit epoch; (2) a single telescope simultaneously observed a transit in two or more wavelengths, producing multiple transit light curves; (3) two or more groups used the same observations to generate different transit light curves and/or made different model fits; and (4) a transit midtime was reported in one timing system (e.g., HJD/UTC) in one work and then was republished later in another timing system (e.g., BJD/TDB). In the first two cases, all of the reported midtimes are independent observations and should be included in timing analyses, but in cases 3 and 4, only one midtime value should be used. Special care needs to be taken with systems that have been repeatedly analyzed, since compilations of compilations often obscure both the source and the original value of the reported transit midtimes.

We checked the midtimes against their references in Ivshina & Winn (2022) for 40 of the 43 UHJs in our full sample (HIP 65 A b, KELT-1 b, and KOI-13 b were not in that work) and found two places where there were duplicated midtimes.

1. For WASP-43 b, each transit from Wang et al. (2021) that also appeared in Patra et al. (2020) and either Gillon et al. (2012) or Murgas et al. (2014) shows up twice in Ivshina & Winn (2022). Since the duplicated transits predate any of the new observations listed in Table 1 in Wang et al. (2021), the listed times must have been sourced from one of the two prior works. Removing the 24 duplicate times from Wang et al. (2021) caused the ΔBIC value to fall by half, and the best-fit curvature went from a tiny but 3σ positive trend with $\dot{P} = (3 \pm 1)$ ms yr^{-1} to less than 1σ from 0 (see Table 7).
2. For WASP-104 b, every transit in both Chen et al. (2021) and Wang et al. (2021) was repeated in the table in Ivshina & Winn (2022). Six transits were removed, and in this case ΔBIC did not change appreciably.

Given the large number of works involved, it is likely there are other instances of duplication in Ivshina & Winn (2022), especially when citing works such as Wang et al. (2021), which do not list the sources of individual transit midtimes. It is important to note that while the impact on ΔBIC of including duplicates is often small, it can be substantial if the duplicated point has very low errors or occurs at a critical point in the sequence. Duplications are also an entirely unnecessary source of error that could be eliminated with better data management practices by the field as a whole. It is recommended that researchers carefully investigate the source of each transit time used in future analyses, particularly before making claims of subtle detections of small effects. For a long-term approach to how the transit timing community could deal with this problem, see our recommendations in Section 8.3.

5.2. Composite Transit Times

We now turn to the related issue of composite transit times, or times that are derived from more than one transit light curve. We have identified at least three potential issues that may arise when attempting to use times derived from more than one transit. (1) Composite times typically have error bars that are much smaller than any individual transit, and they compress all of the timing information into a single point, which can distort ΔBIC analyses of long-term variations. (2) Composite times obscure the source of the original timing and make error detection and correction difficult. (3) Composite times may lead to double-counting transits, if one or more of the individual transits that were used to calculate the composite time were also published on their own.

There are three different ways to produce a composite light curve, some of which may be used in timing analyses with suitable precautions and others that should be avoided. We refer to the three main types as a *stacked midtime*, an *ephemeris midtime* (commonly abbreviated as T_0), and a *weighted-average midtime*.

1. *Stacked transits* result from combining photometric time-series data spanning multiple transit epochs into a single transit light curve. Long photometric time series often have a low signal-to-noise ratio or low sampling for individual transits, and it may not be possible to fit, or even detect, individual transits. By folding on the best-fit orbital period and stacking the data, it is possible to extract a single, higher-quality light curve. Stacked transits are common in discovery papers from large ground-based surveys, as well as for detecting very small

Table 5
Midtime and $O - C$ Values for All Transits Used for Six Planets[a]

Planet	Epoch	Time System	$T_{\rm mid}$	$T_{\rm mid}$ Err. (days)	$O - C$ (days)	Source
CoRoT-2 b	−594	BJD_TDB	2453566.49875	0.003	0.01658384	Rauer et a. (2010); Ivshina & Winn (2022)
CoRoT-2 b	−582	BJD_TDB	2453587.39975	0.003	0.00161869	Rauer et a. (2010); Ivshina & Winn (2022)
CoRoT-2 b	−209	BJD_TDB	2454237.5345	0.0017	−0.00154782	This work
CoRoT-2 b	−208	BJD_TDB	2454239.27859	0.00029	−0.00045492	This work
CoRoT-2 b	−207	BJD_TDB	2454241.0222	0.00024	0.00015799	This work

Note.
[a] Midtimes for CoRoT-2 b, TrES-1 b, WASP-12 b, WASP-19 b, WASP-46 b, and WASP-121 b.

(This table is available in its entirety in machine-readable form in the online article.)

planets in Kepler/K2 data (e.g., Adams et al. 2021). Kepler-1658 b, for instance, is only robustly detected by stacking all transits within an individual Kepler quarter or TESS sector (Vissapragada et al. 2022). In principle, there is no issue with using a midtime that was fit to a stacked transit, provided the data being stacked came from a single origin (e.g., the same ground-based survey) and have roughly consistent noise levels and systematics. It is common practice to assign the midtime of the stacked transit to either the first transit epoch in the sequence or the transit epoch nearest to the sequence midpoint. Often, though, particularly for survey discovery data, the assigned midtime for a stacked transit may not be published, except as it may contribute to the fitted value for an ephemeris midtime (T_0), discussed next.

2. *Ephemeris midtimes*, or T_0, are the result of fitting a set of individual transit midtimes to the linear ephemeris in Equation (2) and may be variously called the reference midtime, the time of conjunction, the time of transit, or similar. In some cases, T_0 is the only timing information provided in a published work. Although it should be common practice to publish the photometric time series for each transit light curve, many papers still do not do so. Nor do papers always report fitted midtimes for each transit light curve. For systems with sparse data, an ephemeris midtime may be one of the few timing points available, and frequently the midtime at the very first epoch is actually an ephemeris midtime. However, using a T_0 value in combination with midtimes derived from individual transits can be problematic. A T_0 value based on multiple transits taken over many months or years will have a much smaller error bar than any of its component transits, or indeed any individual transit, and thus will serve to anchor the model to the assigned transit epoch. In many cases, this results in a larger value for ΔBIC than would result if the individual transit midtimes and errors had been used instead.
3. The third type of composite time is a *weighted-average* time, where two or more midtimes from independent observations (say, transits at two different telescopes) are averaged together. We do not recommend publishing or using weighted-average times, since timing models can easily deal with multiple data points at the same epoch. Moreover, it is impossible to reconstruct an individual midtime and error from a weighted average, which also makes it impossible to assess for mistakes in timing system conversion or sometimes even to determine which transits were used to calculate the average time.

5.2.1. Some Examples of Composite Times in This Work

In Section 6.4, we discuss WASP-121 b, where a single composite point, in this case an ephemeris time, is primarily responsible for the nonzero ΔBIC value. In that case, we do not have access to either the individual times or the associated light curves that were used to calculate T_0, making its impact hard to evaluate.

CoRoT-2 b, meanwhile, contains an example of a stacked midtime. The time series from the CoRoT satellite mission encompasses 82 consecutive, high-quality individual transits, but the data were first published as a single stacked midtime assigned to the midtime of the first transit, with $T_{\rm mid} = 2454237.53562 \pm 0.00014$ [BJD] (Alonso et al. 2008). In this work, we reanalyzed the original photometry so that we could individually fit each of the 82 transits (see Table 5), which had an average error of −0.00020, +0.00023 days in the timing of each transit (50% larger than the error assigned to the single stacked midtime). In an experiment, we found significant shifts in the preferred ephemeris model using the stacked midtime rather than the 82 individual midtimes: ΔBIC fell from 33 to −2, and $\dot{P}$ went from 2σ positive curvature to negative curvature that is indistinguishable from 0. In this particular case, since each of the individual transits could be well fit to a light-curve model on its own, there is no need to use a stacked transit midtime.

We also found that the CoRoT-2 b mission data were being double-counted in Ivshina & Winn (2022). Both the stacked composite time (derived from all 82 transits) from Alonso et al. (2008) and 79 of the 82 individual transit light curves are included in the table in Ivshina & Winn (2022). This duplication had two causes. (1) The individual transit midtimes came from Öztürk & Erdem (2019), who did not analyze the first three transits taken at the longer 512 s cadence; but since the stacked transit was assigned to the midtime of the first (omitted) transit, it appeared to be at a unique epoch. (2) A typo in Ivshina & Winn (2022) caused the omission of the ">1" tag to indicate that the Alonso et al. (2008) time was derived from more than one transit. In this case, double-counting the CoRoT data had only a modest downward effect on ΔBIC (decreasing it by 6).

5.3. Some Words of Caution on Timing Systems

Eastman et al. (2010) provide a thorough discussion of the various timing systems in use in modern astronomy. Briefly, to remove the effects of both the motion of the Earth around the Sun and the motion of the Sun around the solar system barycenter, a dynamical time system must be used to avoid

introducing cyclical variations in an astronomical time series. The recommended standard for reporting exoplanet transit times is BJD using the TDB scale. Critically, for precise timing analyses, all times must be converted into the same timing system before analysis so as to avoid introducing systematic errors.

Most observational times are originally recorded in JD format in the UTC timescale, hereafter referred to as "JD/UTC," and must be converted to barycentric dates, hereafter "BJD/TDB," using the coordinates of the observatory and the coordinates of the star. However, other timing systems are still in common usage. In particular, the heliocenter has historically been easier to calculate, and many midtimes and transit light curves have been reported in Heliocentric Julian Dates (HJD) in the UTC timescale ("HJD/UTC"). Notably, the ETD still uses HJD/UTC for its summary tables. It is also possible to run across times in the TT system, usually HJD/TT. Both TT and TDB are dynamical timescales with subtly different definitions, and midtimes in BJD/TT differ from midtimes in BJD/TDB by only fractions of a second, which is much smaller than the measured midtime error of any of our transits (or any transit published anywhere in the literature to date). TT and TDB are treated as functionally equivalent for this work.

The difference between the solar system barycenter and the heliocenter is small (no more than a few seconds; Eastman et al. 2010), and BJD and HJD have sometimes been used interchangeably, since almost no transit midtimes are known to better than a few seconds. This practice would reasonable if the times were also both in the same dynamical system—but BJD times are almost always given in the TDB system, while HJD times are usually (though not always) in the UTC system. The difference between UTC and TDB is currently 69.184 s (in 2024). The UTC–TDB offset changes with the irregular addition of leap seconds that depends on the precise rotation of the Earth, and the last leap second was added on 2016 December 31.[9] Thus, it is critical to report the full time system used, and herein lie some difficulties with literature light curves. Often, times are reported as BJD only, with BJD/TDB implied, though occasionally light curves will be reported in BJD/UTC. The table of transits from Ivshina & Winn (2022) reports the timing system used for each light curve, usually either BJD/TDB or BJD without any scale specified. However, not all of the works cited by Ivshina & Winn (2022) have properly identified their timing systems, nor have they always converted between timing systems accurately. We have identified multiple errors in this work (see Sections 6.3 and 6.2) relating to missing or erroneously applied BJD/TDB corrections for data that were compiled by Ivshina & Winn (2022).

For all of our new light curves, we begin with data from the instrument in JD/UTC times and use the astropy.time package to convert to BJD/TDB directly. For ETD light curves, we assume that the times listed in the summary table for each planet have been properly converted to HJD/UTC and apply the correction from UTC to TDB using the same astropy functions. It would be preferable to use the JD times directly from the ETD and convert to BJD, but it is currently not possible to download JD times and observatory coordinates in bulk, and it is impractical to do so by hand for thousands of light-curve times. Thus, while most of our times are in BJD/TDB, the ETD times are in a hybrid HJD/TDB system. This has minimal impact given the size of the ETD midtime errors.

[9] https://www.nist.gov/pml/time-and-frequency-division/time-realization/leap-seconds

5.4. Calculating the Best Linear and Quadratic Ephemerides for Each Planet

Because of the complexity of the data sets involved, our timing analysis took an iterative approach as we identified errors in the source data. We began with the series of transit midtimes and errors from both our own fits (Section 4) and our curated collection of literature times (Section 5). For each system, we then ran the following sequence of calculations:

1. Fit the best linear ephemeris (Equation (2)) and quadratic ephemeris (Equation (3)) to the available midtimes.
2. Calculated the ΔBIC value (Equation (5)) to see which model is preferred. Negative values of ΔBIC indicate a linear ephemeris is preferred, while positive values indicate a quadratic ephemeris is preferred. The sign of dP/dE determines if the system had a period increase (positive dP/dE) or decrease (negative dP/dE). Values of ΔBIC for each planet are shown in Figure 2.
3. Ran a series of omit-one tests, omitting each individual midtime in turn and calculating the resulting ΔBIC. Erroneous midtransit times can significantly impact ΔBIC, particularly if they have very small error bars that act to anchor to a particular model. Individual points whose absence or presence changes ΔBIC by more than 25% were flagged and show up as red diamonds in Figures 3–10.
4. Calculated the rescaled ΔBIC value. Some, though not all, transit midtimes are reported with unrealistically low error bars. The ideal practice would be to refit all literature light curves with the same fit model and method; however, this is usually impractical or impossible, especially for large data sets where the photometry for many light curves has not been published. Instead, we devised a "rescaling test," where we used the χ^2 value of the best linear fit using the original errors and then scaled all error bars up by the same factor, so that $\chi^2 = 1$, then ran a separate fit to the rescaled data. We then calculated the resulting ΔBIC value using the rescaled error bars. Figure 2 shows the impact of rescaling, which almost always decreases the value for ΔBIC, even causing some values to become negative (switching to a preference for a linear ephemeris); however, genuine detections such as WASP-12 b remain highly significant (rescaled ΔBIC = 331 versus original ΔBIC = 936).
5. Investigated outliers, especially those that failed the omit-one test. If any times needed to be removed or altered, we then reran the above.

5.5. Identifying Systems of Interest

We show the ΔBIC values for all 43 systems for which we have observed at least one new transit in Figure 2. We chose ΔBIC > 30 as a somewhat arbitrary threshold to investigate a small number of systems with the highest likelihood of a changing ephemeris. (See Section 6.8 for a discussion of this threshold.) We discuss below the timing results for four planets, including WASP-12 b, that still meet our ΔBIC > 30 criteria, as well as two planets, CoRoT-2 b and WASP-19 b,

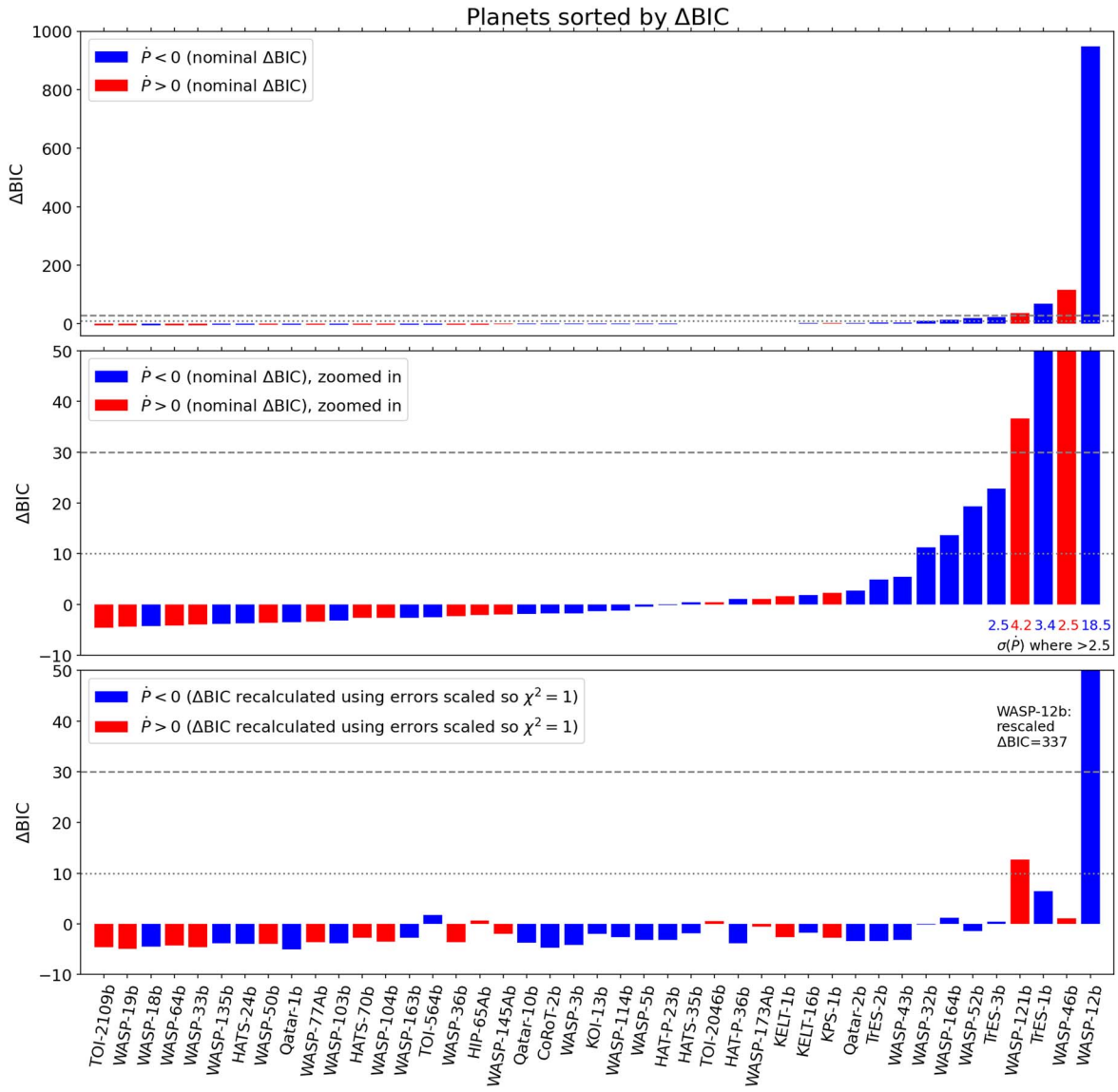

Figure 2. ΔBIC values for 43 planets for which we report at least one new light curve. All panels: positive ΔBIC values indicate that a quadratic model is preferred over a linear model. Negative values of $\dot{P}$ (decreasing orbital periods) are shown in blue and positive $\dot{P}$ (increasing orbital periods) in red. Two horizontal lines show arbitrary cutoffs at ΔBIC = 30 (dashed) and 10 (dotted). Top panel: nominal ΔBIC values (Table 7) with WASP-12 b clearly standing apart from the other planets. Middle panel: same data as top, but zoomed in to show all four systems with ΔBIC $\geqslant$ 30 (WASP-121 b, TrES-1 b, WASP-46 b, and WASP-12 b). These four systems also all have at least marginally significant ($\geqslant 2.5\sigma$) values for $\dot{P}$, with σ values plotted below the bar. Bottom panel: recalculated values of ΔBIC using error bars on all points that have been uniformly rescaled so that the χ^2 value of the fit is equal to 1 (see description of the rescaling test in Section 5.4). Few planets retain positive ΔBIC values, indicating that in many cases high nominal ΔBIC values may be due to underestimated errors.

whose initially promising ΔBIC values ultimately proved to result from errors in the literature.

6. Timing Analysis Results for Individual Systems

6.1. WASP-12 b: Solid Detection of Decreasing Orbital Period

Timing data for the planet with the clearest case for orbital decay, WASP-12 b (Patra et al. 2017; Baluev et al. 2019; Yee et al. 2020), with $P = 1.09$ days, are shown in Figure 3. Six new full or partial transits were observed with IoIO for this project in 2022–2023 (Table 1). We also fit two sectors of TESS data (Sector 44 and Sector 45) that were released after the analysis of Ivshina & Winn (2022), which had Sector 20 and Sector 43. We used 145 light curves from the literature as compiled by Ivshina & Winn (2022), plus 28 additional, nonduplicated light curves from the ETD (requiring midtime errors of less than 5 min and DQ = 1; Poddaný et al. 2010). The best-fit parameters for linear and quadratic ephemerides are shown in Table 6. Despite the modest precision of the new data (due mostly to unfavorable weather), our value for $\dot{P} = -29.8 \pm 1.6$ ms yr^{-1} is quite similar to previously published values, e.g., -29 ± 2 ms yr^{-1} from Yee et al. (2020).

6.2. WASP-19 b: No Evidence for Orbital Decay

WASP-19 b, discovered in Hebb et al. (2010), has one of the shortest orbital periods for a UHJ at just under 0.79 day, and as such has long been viewed as a promising target for orbital decay. It also has one of the longest observational baselines, with data spanning 15 yr and nearly 7000 epochs (Figure 4). Only upper limits on orbital decay were found by Petrucci et al. (2020) and Rosário et al. (2022), though a weak 3σ period

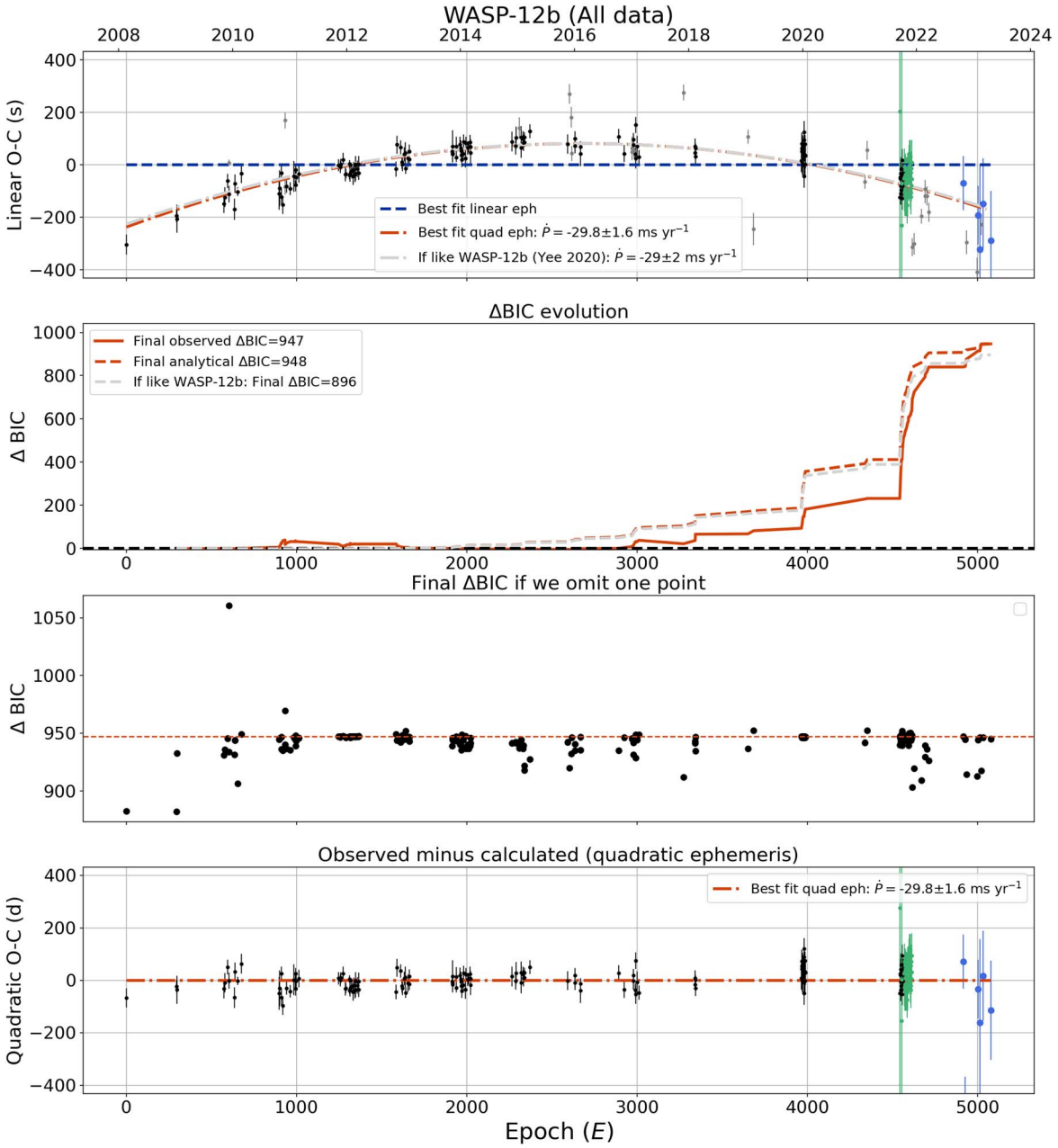

Figure 3. Timing results for WASP-12 b. Panels are listed from top. Panel (1): observed minus calculated times assuming a linear ephemeris. Midtimes derived from light curves that we fitted are in green (TESS) and blue (new ground-based observations). Literature midtimes compiled by Ivshina & Winn (2022) are in black, while those from the ETD are in gray. If there were critical points from the third panel, they would also appear as red diamonds. Panel (2): ΔBIC from observations (solid orange line) and from analytical calculation assuming our value of $\dot{P}$ (dashed orange line; see Jackson et al. 2023). The expected evolution of ΔBIC if $\dot{P} = -29.7$ ms yr^{-1}, as for WASP-12 b in Yee et al. (2020), is shown by the gray dashed line, with its final value noted in the legend. Panel (3): final ΔBIC using all data (dashed orange line), compared to the final ΔBIC if just one point were omitted. If there are any points that lead to large shifts (final ΔBIC changes by ⩾25% and at least 5), they are highlighted with red diamonds in panels one and three. Panel (4): observed minus calculated times for the best-fit quadratic ephemeris.

decrease detection was reported by Ivshina & Winn (2022). These prior works have made it clear that if WASP-19 b is decaying, it must be doing so at least an order of magnitude more slowly than WASP-12 b, and consequently, $Q'_\star$ must be at least an order of magnitude larger ($\geqslant 10^6$).

Our analysis includes two new transits from the SAAO 40 inch in 2022, as well as two newly fit sectors of TESS data (Sectors 62 and 63), for a total of 74 new transit midtimes.

We started with 141 literature times for WASP-19 b listed in Ivshina & Winn (2022). Two points were rejected for having errors greater than five minutes. We then identified 10 times from Cortés-Zuleta et al. (2020) that were not included in Ivshina & Winn (2022), of which we omitted two: one had midtime error greater then five minutes, and the other is a non-obvious duplicate. The duplicate was found in Table A.5 of Cortés-Zuleta et al. (2020) where two nominally different epochs are reported at E=-2063 and $T_{\rm mid}$ = 2454775.3372 from Hebb et al. (2010) and E=-2061 and $T_{\rm mid}$ = 2454776.91566 from Anderson et al. (2010). On closer examination the midtime at E=-2061 is derived from a joint analysis of an occultation observed on 2009 May 3 by Anderson et al. (2010) and the same transit light curve from

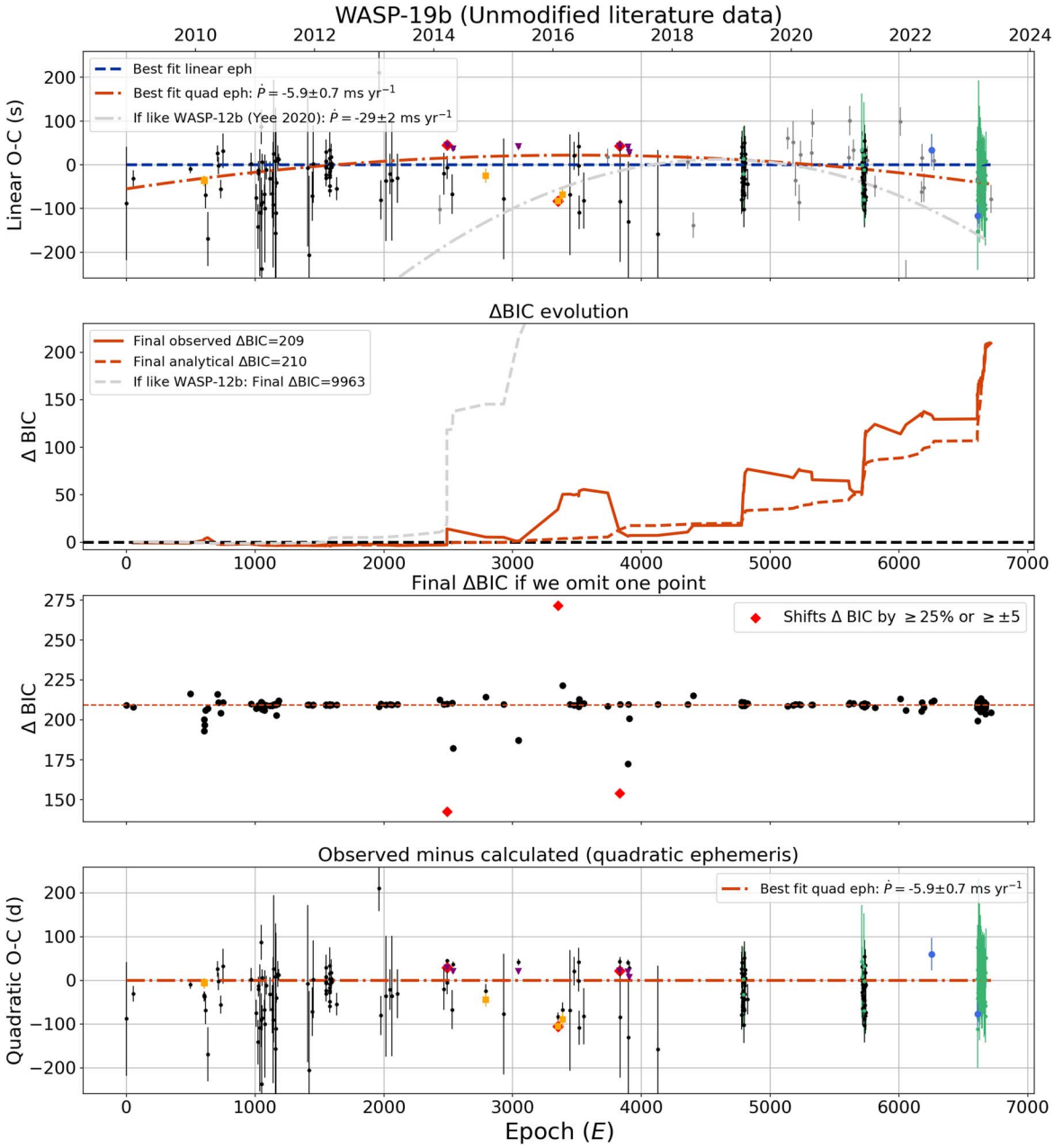

Figure 4. Timing results for WASP-19 b using unmodified literature times, as discussed in Section 6.2. The description of the data is the same as in Figure 3, except that times from three works are highlighted: six transits from Espinoza et al. (2019), which appear as purple triangles, center; three transits from Tregloan-Reed et al. (2013), which appear as a single orange square, left; and three transits from Sedaghati et al. (2017), which appear as orange squares, center. These works all either have errors or are responsible for critical points that strongly affect ΔBIC; see discussion in the text.

2008 Nov 11 from Hebb et al. (2010) that was reported at E=-2063, and thus does not represent an independent midtime measurement. (Occultation timing analysis is beyond the scope of the present work.) We also downloaded 84 midtimes from the ETD (through 2024 Feb). Of these, 34 midtimes had DQ=1 and errors less than five minutes (Poddaný et al. 2010). This number was reduced to 29 unique transits after removing two midtimes that were entered from the literature (Hebb et al. 2010; Dragomir et al. 2011), two midtimes from light curves that were later reanalyzed and published by Petrucci et al. (2020) and then Ivshina & Winn (2022), and one identical duplicate in the ETD table. Our total number is thus 176 literature midtimes.

We then made three small modifications to the literature record. (1) We restored an extra significant figure to the values from Ivshina & Winn (2022), which were rounded to five places, using the original values published in Petrucci et al. (2020). This avoids misidentifying as duplicates a few transits with very similar midtimes that were observed in multiple filters by the same instrument and otherwise does not impact results. (2) For one transit originally published by Espinoza et al. (2019), we made a different choice than Ivshina & Winn (2022) about which of several published midtimes to use. All six transits published by Espinoza et al. (2019) also appear with identical values and errors in Patra et al. (2020) after converting to BJD/TDB, but just one appears, nonidentically, in Petrucci et al. (2020) where the light

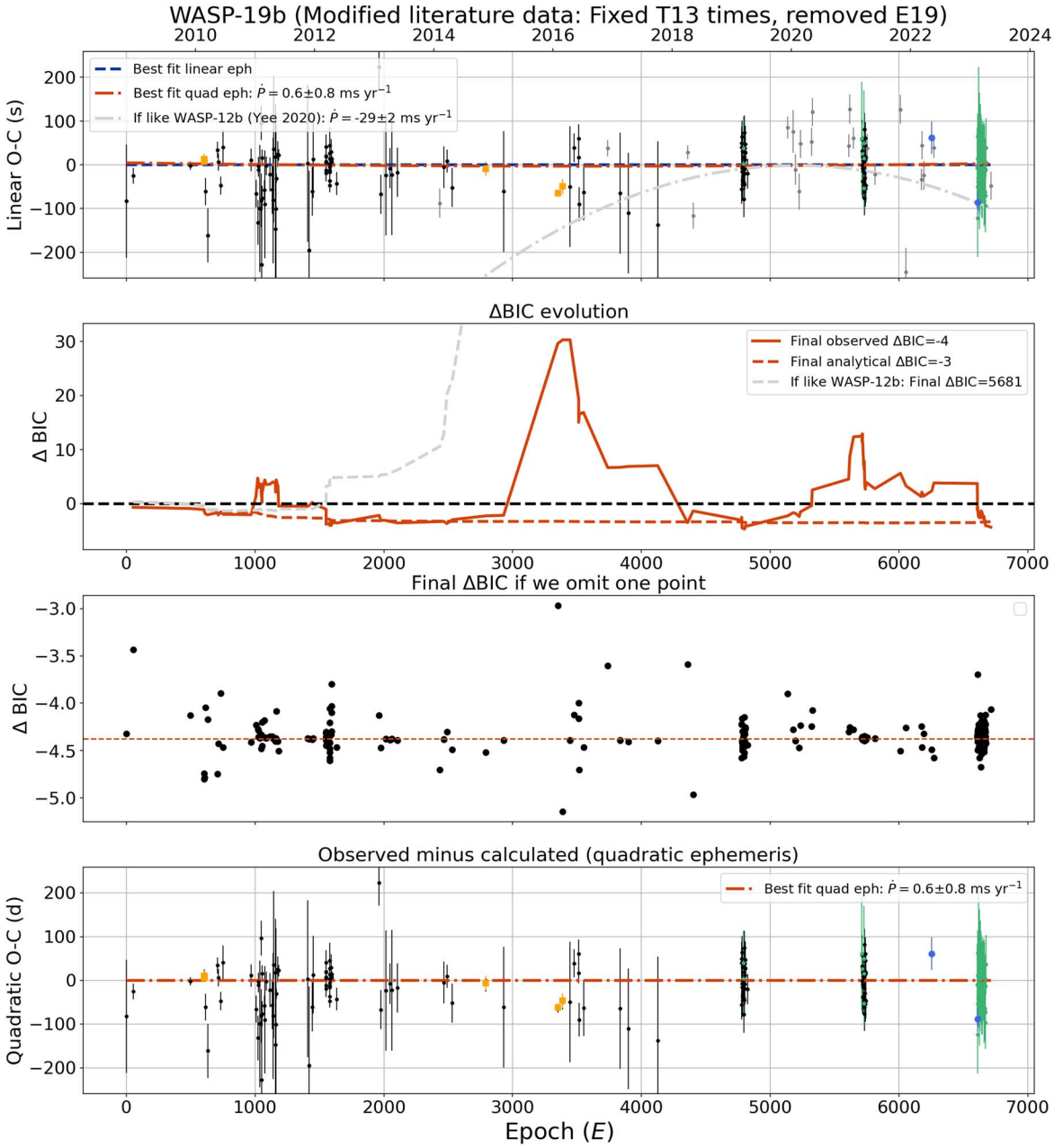

Figure 5. Timing results for WASP-19 b using the modified literature times, as discussed in Section 6.2. Description of the data is the same as Figure 3, except that times from two works are highlighted: three transits from Tregloan-Reed et al. (2013), which appear as a single orange square at left, and three transits from Sedaghati et al. (2017), which appear as orange squares at center. Note that the timing for three transits from Tregloan-Reed et al. (2013) have been corrected and six transits from Espinoza et al. (2019) have been removed, compared to Figure 4. Meanwhile, the times from Sedaghati et al. (2017) are no longer critical points that strongly impact the fitted value for ΔBIC. See discussion in the text.

curve was reanalyzed; this was the value that appeared in Ivshina & Winn (2022). The difference between the two midtimes in question is 26 seconds, and Petrucci et al. (2020) also found much higher error bars (13 s vs. 4 s). As only one of the six Espinoza et al. (2019) transits was reanalyzed by Petrucci et al. (2020), and since the Espinoza et al. (2019) times are critical points for the ΔBIC analysis (about which more soon) we made the decision to treat the six transits consistently and used all six BJD/TDB midtimes as published in Patra et al. (2020). (3) For the three times from Sedaghati et al. (2017), we swapped in the original values and errors for the ones that Petrucci et al. (2020) published using refit light curves and which are used by Ivshina & Winn (2022). The midtime values were nearly the same, but two of the three light curves have notably smaller error bars in Petrucci et al. (2020), especially the transit $T_{\rm mid} = 2457448.71294 \pm 0.00020$ in the original versus the refit $T_{\rm mid} = 2457448.71292 \pm 0.0000766$—less than 2 sec difference in midtime but a factor of three smaller error. We have chosen to use the larger error as the more conservative choice, although the ultimate effect on ΔBIC after correcting the other issues noted below is minimal.

Using the essentially unmodified literature data as just described we find ΔBIC = 209, which is quite high, with a statistically significant $\dot{P} = -5.9 \pm 0.7$, a nominal 8σ detection (see Figure 4). However, closer inspection reveals several

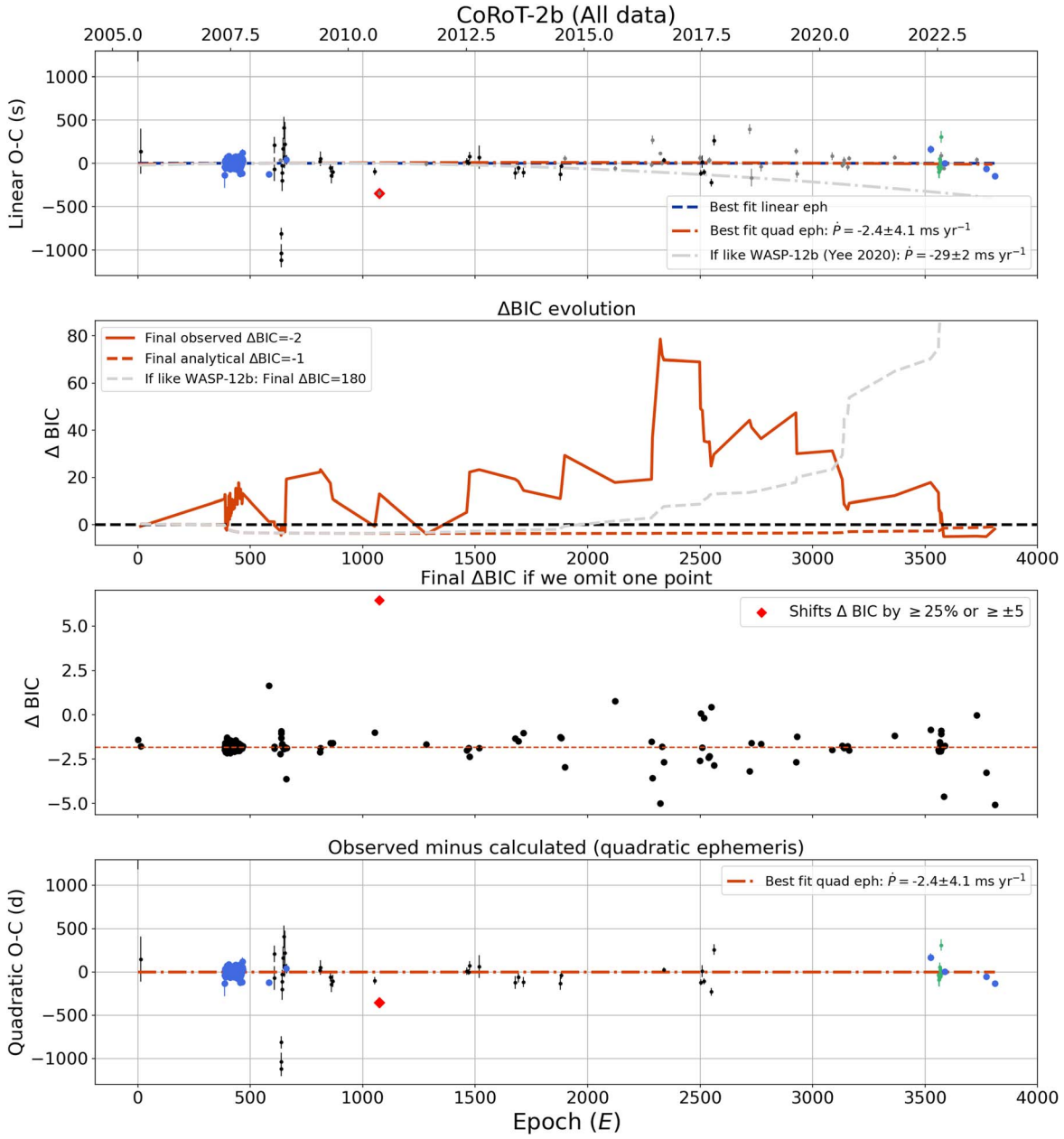

Figure 6. Timing results for CoRoT-2 b with new fit values for CoRoT mission data replacing the values used by Öztürk & Erdem (2019) and Ivshina & Winn (2022). Instead of a strong negative curvature, CoRoT-2 b shows no signs of nonlinearity. The description of the data is the same as in Figure 3.

issues that bring this result into doubt, which we will now discuss in more detail, along with the impact of each on the calculated ΔBIC value.

1. First, we found an apparent timing conversion error in Tregloan-Reed et al. (2013), which has since been propagated to other works, including Patra et al. (2020) and Ivshina & Winn (2022). Two tables in Tregloan-Reed et al. (2013) contain timing information, with their Table 2 listing the fitted midtimes for three transit light curves in HJD/UTC and their Table 4 converting to HJD/TDB for direct comparison with other works. At the observation epoch the difference between these two time systems should be about 66 seconds (accounting for both leap seconds and the TAI constant offset), but the actual differences between the listed midtimes are 41 s, 33 s, and 38 s. The cause for this difference is unknown, but may be an incomplete timing conversion, where either the leap seconds or the TAI offset were included, but not both. Using the online tool from Eastman et al. (2010)[10] to directly convert the times in their Table 2 from HJD/UTC to BJD/TDB, we find values of 2455251.797060, 2455252.585840, and 2455255.741230, which are used in all subsequent analyses. The uncorrected points are highlighted in Figure 4 as the orange squares around E = 600. Fixing the timing of these three points alone caused a 25% drop to ΔBIC = 147.
2. After correcting the timing for the three times from Tregloan-Reed et al. (2013), the strength of the ΔBIC value rests on three points which fail our omit-one test;

[10] https://astroutils.astronomy.osu.edu/time/hjd2bjd.html

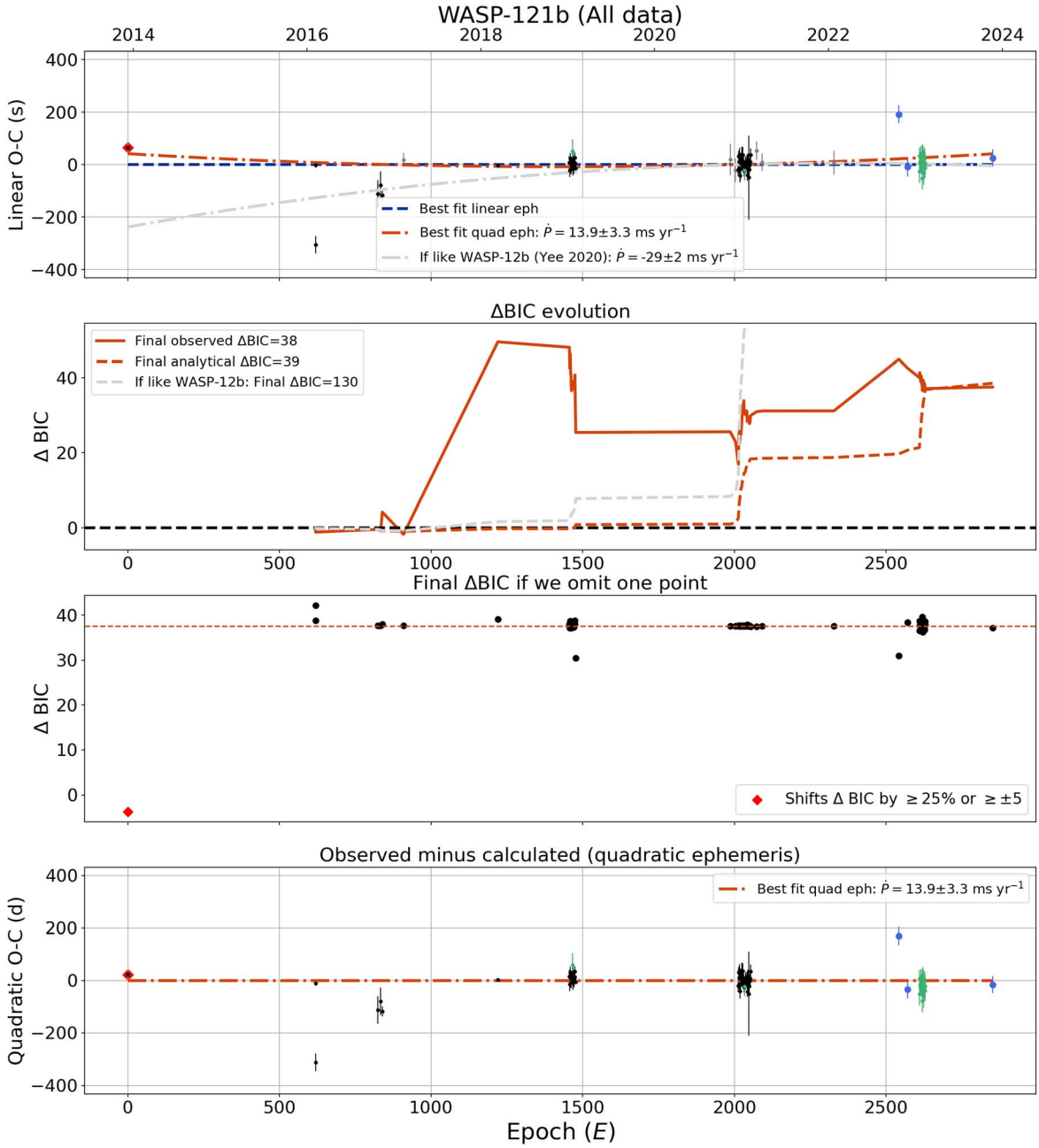

Figure 7. Timing results for WASP-121 b. The description of the data is the same as in Figure 3.

removing each point individually changes the ΔBIC value for the system by 30%. Two of these times are among the six transits discussed above from Espinoza et al. (2019). These transits were white light transits created by combining high-resolution spectroscopic observations with the 6.5 m Magellan telescope using IMACS, and were of such high precision that even with visible spot crossings during transit the timing precision was between 4–9 s in the original work. Besides the low errors, all six points from Espinoza et al. (2019) appear above the line for the best linear ephemeris by about a minute (see the purple triangles in Figure 4). It is worth noting that while at first glance this might appear to be a UTC/TDB conversion error, we have not found any definitive evidence to support that hypothesis. The values in Espinoza et al. (2019) were published in BJD/UTC, as confirmed by correspondence with the authors of that work, and apparent differences between the values in Espinoza et al. (2019) and subsequent works are due to correctly converting the original midtimes to BJD/TDB. The source of the apparent universal offset is thus still unknown. In combination, the very low errors and the consistent offset are entirely responsible for all of the remaining ΔBIC. We explored two approaches to dealing with this issue:

a. Increasing the errors on the six points from Espinoza et al. (2019). Noting that the single transit that was refit by Petrucci et al. (2020) had three times the fitted error as that reported by Espinoza et al. (2019), we tripled the error bars on all six transits and recalculated the value of ΔBIC. This caused a drop to insignificance, with $\Delta\mathrm{BIC} = -3$ and $\dot{P} = -0.8 \pm 0.7$.

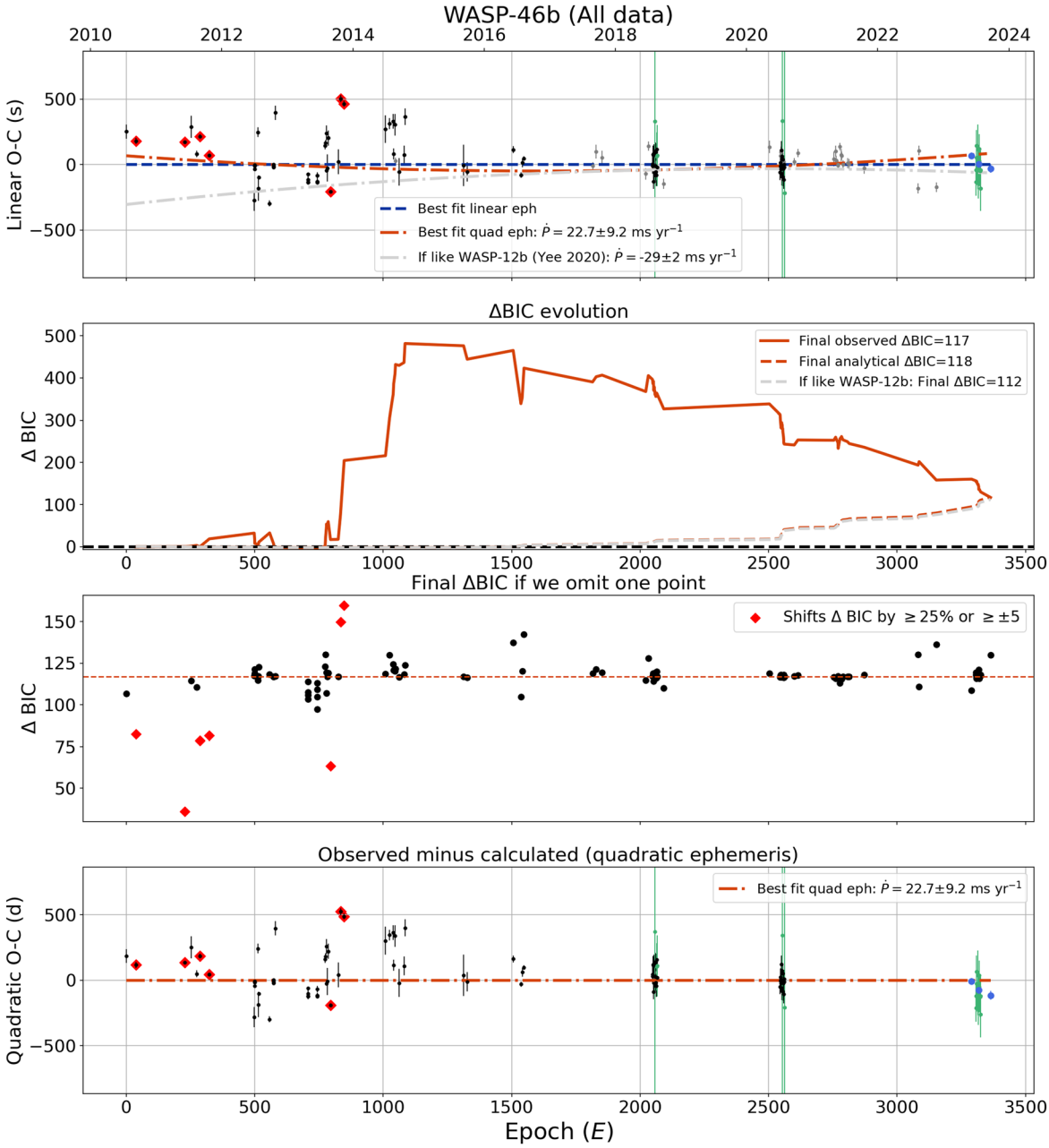

Figure 8. Timing results for WASP-46 b. The description of the data is the same as in Figure 3.

However, one of the Sedaghati et al. (2017) points remains an outlier in this approach.

b. Removing the six points from Espinoza et al. (2019). This also causes the effect to vanish with $\Delta\mathrm{BIC} = -4$ and $\dot{P} = 0.6 \pm 0.8$, a strong preference for a linear ephemeris (Figure 5). In addition, with this approach there are no critical times that affect the ΔBIC value by more than 25%. This is the version we adopted as preferred and which will be used in subsequent analyses in this paper.

With these modifications to the literature times, we find that decay, if it is happening for WASP-19 b, is proceeding at an as-yet undetectable pace (Figure 5).

6.3. CoRoT-2 b: No Orbital Decay

CoRoT-2 b, with $P = 1.74$ days, was the second planet announced by the CoRoT space mission (Alonso et al. 2008), and it has one of the longest baselines in our survey, with data spanning 18 yr (Table 3). Prediscovery data using BEST show clear indications of transits 2 yr before the CoRoT discovery, though only one of those light curves spanned both ingress and egress (Rauer et al. 2010). This planet has been frequently studied, since in addition to being one of the earliest known transiting planets, it orbits a highly active (7%–20% of the surface covered in spots; Guillot & Havel 2011), rapidly rotating ($P_{\rm rot} = 4.5$ days), likely young (30–300 Myr) star (Gillon et al. 2010), and the planet itself has an inflated radius ($R_p = 1.5\ R_{\rm J}$ and $M_p = 3.3\ M_{\rm J}$) that is a challenge to reproduce

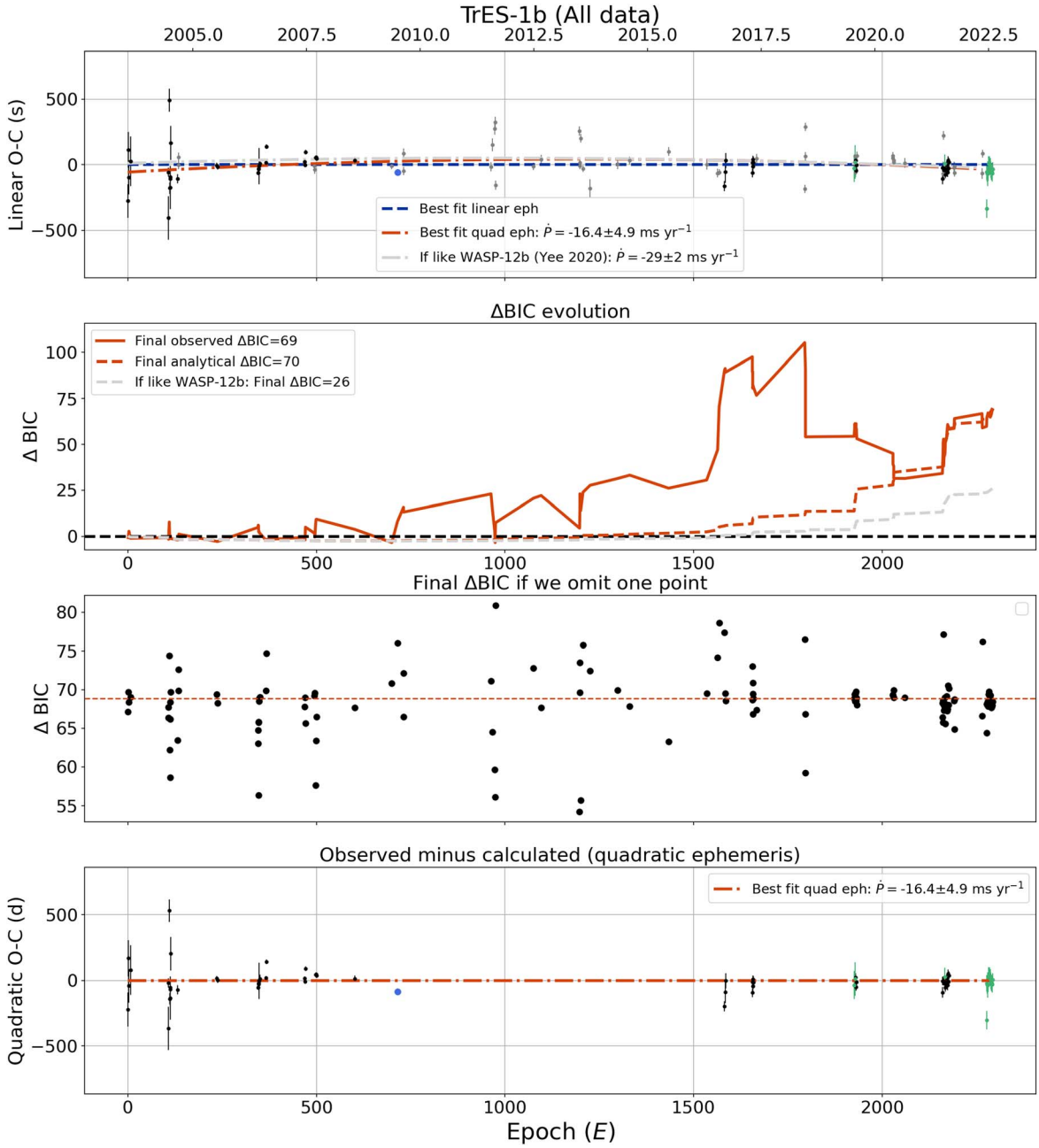

Figure 9. Timing results for TrES-1 b. The description of the data is the same as in Figure 3.

theoretically (Gillon et al. 2010). Previous work has found suggestions of nonlinearity in the ephemeris: Öztürk & Erdem (2019) measured $\dot{P} = -8 \pm 3$ ms yr^{-1}, though with BIC values that favor a linear model, while Ivshina & Winn (2022), using additional data from TESS, found a much higher $\dot{P} = -104 \pm 6$ ms yr^{-1}. In both cases, high scatter was seen in the timing residuals. Recently, Wang et al. (2023) found that the tiny error bars reported in Öztürk & Erdem (2019) strongly influenced the values for $\dot{P}$; using more realistic errors, they found a significantly decreasing period with $\dot{P} = -22 \pm 3$ ms yr^{-1} between the two previous estimates.

We report seven new full or partial transits: three observed in 2008 (Adams 2010), three observed in 2022–2023 with the SAAO 40 inch telescope, and one observed in 2023 with MINERVA-Australis. We have also fit 12 TESS transits from Sector 54, which was released after the publication of Ivshina & Winn (2022). Finally, we have refit the original CoRoT mission data, which observed 82 consecutive transits between 2007 May and October. We include in our timing analysis the reported transit midtimes for 36 light curves from the literature, as compiled by Ivshina & Winn (2022) after omitting duplicates and one composite time, plus 29 additional, nonduplicated light curves from the ETD, requiring midtime errors of less than 5 min and DQ = 1 (Poddaný et al. 2010). Such a large and diverse data set is very useful for highlighting the challenges that arise with long-term timing analyses. We describe the case of CoRoT-2 b in detail to illustrate how more than one kind of error can coexist in the same data set and to illustrate the detective work that is required to both identify and fix the errors.

Our initial examination of the system added the seven new ground-based transits plus TESS Sector 54 to the midtimes

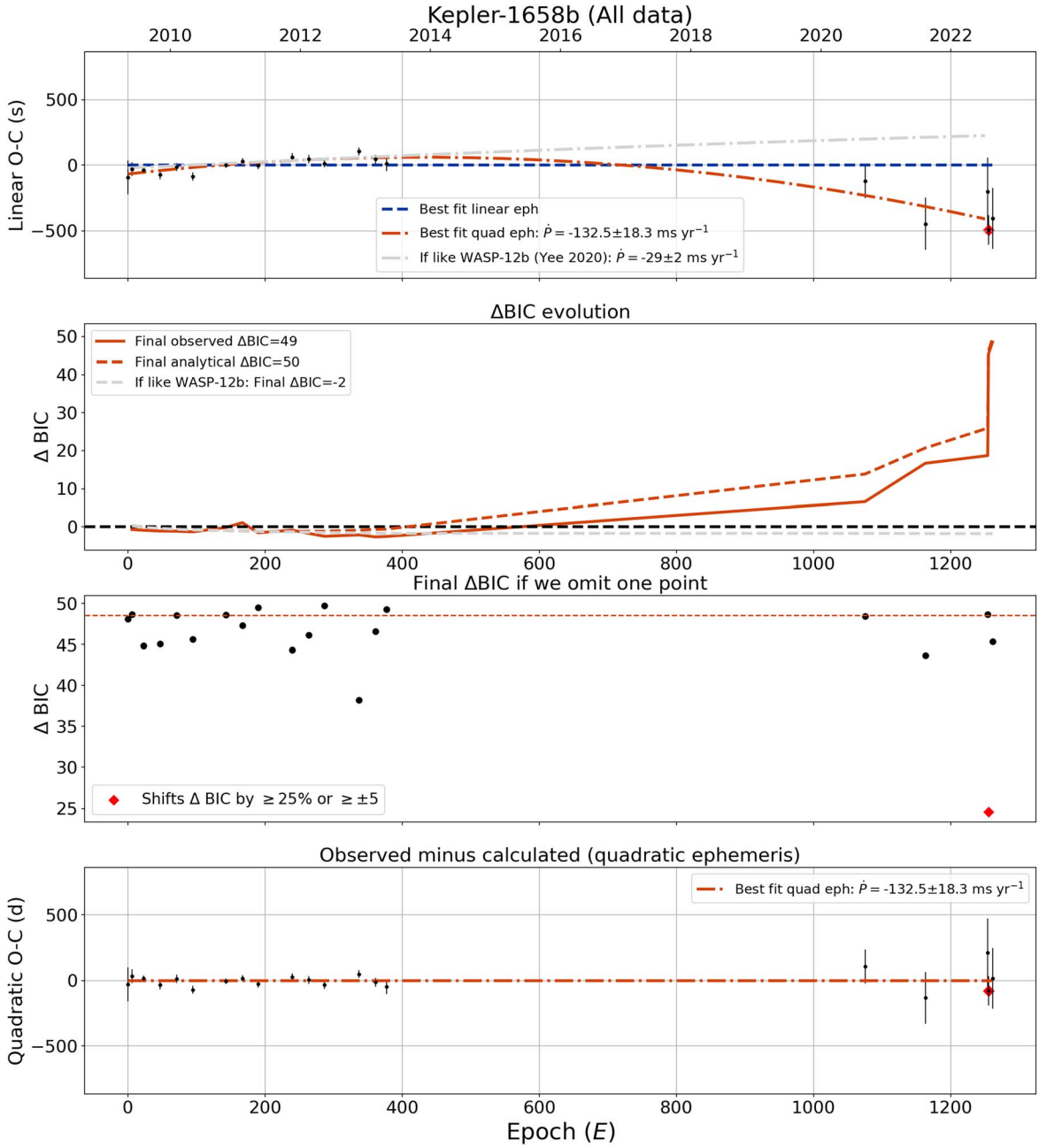

Figure 10. Timing results for Kepler-1658 b, using data from Vissapragada et al. (2022). The description of the data is the same as in Figure 3.

collected by Ivshina & Winn (2022) but did not reanalyze the CoRoT mission times. Using these data, CoRoT-2 b had the second strongest signature for a nonlinear orbital period in our sample (after WASP-12 b), with a 3.1σ detection of a decreasing period and a ΔBIC value of 383. The initial best-fit rate of decay was calculated to be $\dot{P} = -29.4 \pm 9.5$ ms yr^{-1}. This value was consistent with what Öztürk & Erdem (2019) reported and would have implied a very low value for $Q'_\star < 10^4$, and thus we subjected the data to additional scrutiny.

Three issues were noted right away.

1. *An outlier.* One point from the ETD caused the ΔBIC value to change by ±100. This was found to be an error in the summary table on the ETD website, which incorrectly reported the JD, rather than HJD, time of observation, as became apparent when consulting the individual transit details page.[11] We have corrected the midtime in our analysis, as well as in Table 5; however, we caution that it is likely that such a large database as the ETD contains other similar errors.
2. *Underestimated errors.* The second issue involves the published times for the CoRoT mission data from Öztürk & Erdem (2019). The CoRoT mission discovery data set contains 82 consecutive, high-quality transits at the very beginning of the time series and is highly influential on the observed ΔBIC value. However, the errors on individual transit midtimes reported in Ivshina & Winn (2022) and originally published in Öztürk & Erdem (2019) were much

[11] http://var2.astro.cz/EN/tresca/transit-detail.php?id=1343557668, last accessed 2023 October 13.

Table 6
Best-fit Transit Ephemerides for Six Planets

Decreasing Orbital Periods		
Parameter	WASP-12 b	TrES-1 b[a]
ΔBIC	947.1	68.8
Linear P (days)	$1.09141892 \pm 0.00000005$	$3.03006986 \pm 0.00000010$
Linear $T_{\rm mid}$	$2457800.69944 \pm 0.00008$	$2457868.26528 \pm 0.00010$
Quad. P (days)	$1.09141858 \pm 0.00000004$	$3.03006915 \pm 0.00000023$
Quad. $T_{\rm mid}$	$2457800.70032 \pm 0.00007$	$2457868.26561 \pm 0.00014$
Quad. dP/dE	$(-1.031 \pm 0.056) \times 10^{-11}$	$(-1.576 \pm 0.47) \times 10^{-9}$
$\dot{P}$ (ms yr^{-1})	-29.8 ± 1.6	-16.4 ± 4.8
σ ($\dot{P}$)	18.5	3.4
$Q'_\star$	1.6×10^5	1.6×10^2
Lifetime (Myr)	3.2	16.0
Increasing Orbital Periods		
Parameter	WASP-46 b	WASP-121 b
ΔBIC	116.8	37.6
Linear P (days)	$1.43037298 \pm 0.00000014$	$1.27492474 \pm 0.00000007$
Linear $T_{\rm mid}$	$2458343.17327 \pm 0.00020$	$2459223.80556 \pm 0.00005$
Quad. P (days)	$1.43037343 \pm 0.00000023$	$1.27492508 \pm 0.00000010$
Quad. $T_{\rm mid}$	$2458343.17281 \pm 0.00027$	$2459223.80557 \pm 0.00005$
Quad. dP/dE	$(1.027 \pm 0.42) \times 10^{-9}$	$(5.6 \pm 1.3) \times 10^{-10}$
$\dot{P}$c (ms yr^{-1})	22.7 ± 9.1	13.9 ± 3.3
σ ($\dot{P}$)	2.5	4.2
Constant Orbital Periods		
Parameter	CoRoT-2 b	WASP-19 b
ΔBIC	−0.8	−4.4
Linear P (days)	$1.74299709 \pm 0.00000007$	$0.78883900 \pm 0.00000001$
Linear $T_{\rm mid}$	$2454580.90647 \pm 0.00007$	$2458860.73532 \pm 0.00004$
Quad. P (days)[b]	$1.74299728 \pm 0.00000029$	$0.78883902 \pm 0.00000003$
Quad. $T_{\rm mid}$[b]	$2454580.90650 \pm 0.00008$	$2458860.73530 \pm 0.00005$
Quad. dP/dE[b]	$(-1.5 \pm 2.2) \times 10^{-10}$	$(1.4 \pm 1.9) \times 10^{-11}$
$\dot{P}$(ms yr^{-1})	$^{-2.8}_{+3.9}$	0.6 ± 0.8
σ ($\dot{P}$)	0.7	0.7

Note.
[a] With $Q'_\star < 200$, orbital decay is an unlikely explanation.
[b] Best-fit quadratic ephemeris for comparison; use linear ephemeris for prediction.

smaller than the scatter between midtime residuals ($O - C$ values), indicating that the errors were probably underestimated, as noted by Wang et al. (2023). Indeed, Figure 1 in Öztürk & Erdem (2019) shows adjusted transit midtime errors that are ∼10 times higher, though their table (perhaps inadvertently) published the smaller errors. Low error bars on 79 precise points at an early epoch have a huge impact on the ΔBIC value, so correcting these errors was of critical importance.

3. *Strong unexplained trend.* The most serious issue was a trend that was apparent by eye in the 150 days of CoRoT mission data from Öztürk & Erdem (2019). This trend would have implied a faster rate of decay than that of WASP-12 b and $Q'_\star < 10^4$. In contrast to WASP-12 b, for which the star may be slightly evolved (see Section 8), if anything, the evidence points toward CoRoT-2 being a young star, with corresponding high values expected for $Q'_\star$. Removing the CoRoT points entirely caused the ΔBIC value to drop near 0, so it was clear that any apparent detection of orbital period decrease rested on the timing of these transits.

To get to the bottom of both issue 2 and issue 3, we downloaded the CoRoT mission data and refit all 82 transits (see Section 5). Using our new times, which are shown in Table 5, we reran the timing analysis and found that ΔBIC = −2, indicating no orbital decay. Our timing results are shown in Figure 6. The differences between our values for the CoRoT mission times and the midtimes reported by Öztürk & Erdem (2019) range from 200 to 500 s and follow quite closely the expected barycentric correction at each midtime. Thus, we hypothesize that Öztürk & Erdem (2019) used JD times in their light curves instead of either HJD/TT (in the older version of the CoRoT pipeline that they worked with) or BJD/TDB (in the Legacy version used in this work). Unfortunately, this error was then propagated to Ivshina & Winn (2022), who labeled the data as being in BJD/TDB.

6.4. WASP-121 b: Possible Period Increase Heavily Dependent on Single Composite Time at Earliest Epoch

WASP-121 b has $P = 1.27$ days and was discovered by Delrez et al. (2016). We report three new light curves from 2022 to 2023 with the SAAO 40 inch (Table 1) and use an

additional 59 times from the literature and six times from the ETD. The first point in the sequence is a composite of nine high-quality transits taken between 2013 December 9 and 2014 December 29 (Delrez et al. 2016). Note that all but five of the literature times are from two TESS sectors, making this a very sparsely observed target, with large gaps in timing coverage. For that reason, we did not remove the initial composite time, since it would have removed years of timing baseline. Fitting those times individually would provide an excellent constraint on the timing, but unfortunately these data have not been published outside of a figure in the discovery paper.

Our timing analysis is shown in Figure 7. Not surprisingly, the value for ΔBIC is highly dependent on the midtime from Delrez et al. (2016), as shown by the omit-one test; removing it causes the effect to entirely vanish as ΔBIC drops below 0. However, this system is also the only other system (besides WASP-12 b) that does not see its ΔBIC value evaporate when the error bars are rescaled upward (see Figure 2), retaining the second-highest rescaled $\Delta\mathrm{BIC} = 14$ (all data, rescaled errors). This indicates that the system has reasonable error bars on most data but needs additional epochs of observations, through both additional new light curves and a reanalysis, if possible, of the oldest data as individual transit midtimes.

The WASP-121 b system is remarkably poorly sampled in time, with few amateur light curves in the ETD and very little published transit midtime data. Given its possible detection of period increase and its short orbital period, this planet should remain a high priority for future observations.

6.5. WASP-46 b: Evidence for Period Increase Is Murky

WASP-46 b, with $P = 1.43$ days, was discovered by Anderson et al. (2012) and is shown in Figure 8. We observed three new transits in 2023 with the SAAO 40 inch telescope (Table 1) and fit 20 transits from the latest TESS sector (Sector 67). In the timing analysis, we used 86 transit midtimes from Ivshina & Winn (2022; excluding one composite time), which included two sectors of TESS data. We also used 28 nonduplicated light curves from the ETD with DQ = 1 or 2 and errors under 5 minutes.

Several previous timing analyses of WASP-46 b exist, including Ciceri et al. (2016), Moyano et al. (2017), Petrucci et al. (2018), and Davoudi et al. (2021). Since each of these papers also included different subsets of ETD transits, care had to be taken to avoid duplication of data points. No evidence for timing change was seen in Petrucci et al. (2018), though an increase in period was noted by Davoudi et al. (2021). We see a preference for a quadratic model with positive curvature, with $\Delta\mathrm{BIC} = 109$ and a 2.6σ detection of $dP/dE = 21.6 \pm 8.2\ \mathrm{ms\ yr^{-1}}$. However, it is important to note that the data before about 2015 have very high scatter in the transit timing residuals, and seven points have been flagged as outliers that, if omitted individually, cause the value for ΔBIC to range from 32 to 149 (see Figure 2 and 8). No obvious signs of timing conversion errors were found on investigating the source of those early midtimes. We also note that when the errors are rescaled, the value of ΔBIC plummets to 2—still a slight preference for a nonlinear model and among the highest values reported for rescaled ΔBIC values (see Figure 2) but by no means a smoking gun. To resolve this murkiness, we recommend WASP-46 b for further analysis and regular transit observations.

6.6. TrES-1 b: Period Potentially Decreasing, but Orbital Decay Unlikely

TrES-1 b, with a period of $P = 3.03$ days, was one of the first transiting planets discovered (Alonso et al. 2004) and has a very long baseline of observations, as well as prior tentative claims of period decrease (Hagey et al. 2022; Ivshina & Winn 2022). Two transits of TrES-1 b were taken with MORIS on the IRTF in 2009, and we have also fit the two most recent sectors of TESS data (Sectors 53 and 54). We used 61 previously published midtimes from Ivshina & Winn (2022) and another 49 midtimes from the ETD.

In contrast with other systems, no obvious errors were identified in the literature times for TrES-1 b, and none of the midtimes were significant in our omit-one test. We found $\Delta\mathrm{BIC} = 69$ and a 3.4σ detection of $\dot{P} = -16.4 \pm 4.9\ \mathrm{ms\ yr^{-1}}$ (see Figure 9). This is intermediate to, and consistent with, the value of $\dot{P} = -18.36 \pm 3.73\ \mathrm{ms\ yr^{-1}}$ that Ivshina & Winn (2022) found and the value of $\dot{P} = -16.0 \pm 3.76\ \mathrm{ms\ yr^{-1}}$ from Hagey et al. (2022) and less significant than either. However, assuming the apparent period decrease holds up to further observations, the explanation will likely be something other than orbital decay, since the inferred $Q'_\star = 160$ is 5 orders of magnitude lower than the star's predicted $Q'_\star > 10^7$ (Weinberg et al. 2024). Even the rapidly decaying Kepler-1658 b, which orbits a subgiant star, has an estimated $Q'_\star$ value of 10^4, and there are no indications that the star TrES-1 has left the main sequence.

A rapid ephemeris shift could result from perturbations from a massive companion. A stellar companion is located $13\farcs2$ away and is 8.5 mag fainter, though it is not clear if a star that distant could produce a perturbation with the magnitude and minimum oscillation period implied by this detection or if some other as-yet-undetected body would need to be responsible. Exploring the full range of dynamical scenarios that could lead to such a rapid $\dot{P}$ is beyond the scope of this work, but based on our analysis, the signature for a nonlinear period is promising, and we recommend TrES-1 b for continued monitoring.

6.7. Kepler-1658 b: Existing Data Have Promising ΔBIC

We applied our analysis to another promising decay candidate, Kepler-1658 b, a $P = 3.8$ day planet that orbits an evolved host star (2.9 R_S, 1.5 M_S). The orbital period decrease for this planet was measured as $\dot{P} = 131 \pm 22\ \mathrm{ms\ yr^{-1}}$ by Vissapragada et al. (2022). The evolved host star is probably key to explaining the rapid rate of decay: although Weinberg et al. (2024) found that g-mode dissipation is too weak to explain it, Vissapragada et al. (2022) argued that inertial wave dissipation, combined with rapid stellar rotation, could. On the other hand, recent results from Barker et al. (2024) find that the time the star spends with $Q'_\star < 10^4$ may be too short, potentially requiring nonsynchronous rotation if tidal dissipation is to explain the rate of orbital decrease. An alternative explanation could be tidally induced apsidal precession (Barker et al. 2024).

Although we have no new transit observations for this planet due to its very shallow transit depth (0.1%), we applied our analysis pipeline to the midtransit times reported in Vissapragada et al. (2022) as described above. We found $\dot{P} = -132.5 \pm 18.3\ \mathrm{ms\ yr^{-1}}$, with $\Delta\mathrm{BIC} = 49$, in agreement with Vissapragada et al. (2022); see Figure 10. The high scatter in the photometry compared to the depth of individual transits

meant that it was necessary to stack all transits in each Kepler quarter or TESS sector to produce a single time per quarter/sector. In addition, three ground-based observations were made using the Palomar 5.1 m (Vissapragada et al. 2022); one of these points triggers our omit-one test, and without it, the ΔBIC value drops by half. Since this point has low errors and occurs near the end of the sequence, it is not surprising that it holds so much weight; this does not necessarily indicate a problem with the data but does point to the need for additional observations. We note that the nominal and rescaled values for ΔBIC are nearly identical (49 and 50, respectively), indicating that the reported errors are likely reliably measured. The extremely rapid rate of decay for this system means that confirmation could be possible with another year or two of observations.

6.8. Data for Marginal Systems (ΔBIC < 30)

We chose ΔBIC > 30 somewhat arbitrarily to select a handful of the most promising candidates to focus on in this paper. It is also a useful discriminant of where ΔBIC values as calculated with real data and error bars start to become robust enough to have more confidence that they are measuring something other than noise. Many of the systems with possible claimed detections listed in the Introduction were presented at much smaller ΔBIC values. We will now briefly discuss our analysis of the 37 planets that fall below ΔBIC < 30 that have not been described above, as shown in Figure 2. Our preliminary values for ΔBIC < 30 and the best-fit quadratic model parameters are listed in Table 7. We add an important caveat that, unlike with the six main targets of this paper, for these 37 planets, we have *not* done a deep dive into the sources of the literature times used. As we have demonstrated for other systems above, it is quite possible that there may be additional problems lurking in the data for one or more of these systems.

For each of these 37 planets, we used literature times from Ivshina & Winn (2022) and the ETD. We removed duplicate entries and limited the ETD data to DQ = 1 or 2 for most targets. (For WASP-163 b, which has very few ETD points, we allowed all DQ = 1–5, while for Qatar-1 b, TrES-3 b, and WASP-43 b, which have many transits, we used only DQ = 1.) We have not searched for additional transit midtimes that were not in Ivshina & Winn (2022), including systems for which there is known Kepler or K2 data. We have, however, analyzed additional sectors of TESS data where available. For systems that are recently discovered or have very few published literature times, we refit some literature light curves that had not previously had individual fits, using data provided in private correspondence with the authors of those works. These systems are HATS-70 b (six light curves; Zhou et al. 2019), NGTS-1 b (one light curve and one NGTS composite light curve; Bayliss et al. 2018), Qatar-10 b (seven light curves; Alsubai et al. 2019), and WASP-43 b (three light curves; Fox & Wiegert 2022). These analyses will be part of forthcoming publications similar to this one, and the values presented in Table 7 should be considered preliminary results.

For all systems with nominal ΔBIC < 30, few retained a positive value for ΔBIC when we rescaled the error bars to determine the impact of underestimated errors on ΔBIC (see discussion of test in Section 5.4). Of the four high-ΔBIC (ΔBIC > 30) planets, all still have positive rescaled ΔBIC values, as noted above. But among the four intermediate planets (10 < ΔBIC < 30), only two, WASP-164 b and TrES-3 b, still have positive rescaled ΔBIC values, and among the eight planets with slightly positive nominal values (0 < ΔBIC < 10), just one, TOI-2046 b, is still positive in the rescaled test. Two other planets, TOI-564 b and HIP 65 A b, had small negative nominal ΔBIC values that switched to small positive rescaled ΔBIC values. The last three planets are all sparsely sampled with large errors on individual transits and only 4–5 yr of baseline, precisely the kinds of systems where swings in ΔBIC are common (Jackson et al. 2023), and more data are needed before the true patterns of these systems will become clear. We interpret the shifts in ΔBIC to be suggestive that underestimated errors alone may explain most of the marginal detections of decreasing orbital period, both here and in the literature.

Of the four planets in Figure 2 with intermediate values of 10 < ΔBIC < 30, TrES-3 b, WASP-52 b, WASP-164 b, and WASP-32 b, all have decreasing periods, though none have significant values of $\dot{P}$ ($1.6 < \sigma \leqslant 2.5$). Of these, two have previous claimed detections. (1) A possible decreasing period for TrES-3 b has been noted at similar marginal levels by other works (Hagey et al. 2022; Mannaday et al. 2022). Given that TrES-3 b is a long-studied planet around a bright star with particularly deep transits, hundreds of diverse light curves have been recorded by amateurs and professionals alike (with over 600 light curves listed in the ETD alone), making the chance of there being undetected mistakes in the literature high. A thorough reanalysis of the available record needs to be undertaken before any claims for or against period change could be credibly believed for TrES-3 b. (2) Sun et al. (2023) noted possible nonlinearity for WASP-32 b, though that work preferred an apsidal precession model to the quadratic orbital decay model. Neither their value for $\dot{P}$ nor ours is significant (both around 2σ), and the system is relatively sparsely observed. Additional observations are required to assess this claim.

7. Preliminary Population Analysis: Where Are the Decaying UHJs?

7.1. Observational Constraints: In What Systems Could We Even Detect WASP-12 b–Like Decay?

Most UHJs in our sample prefer a linear ephemeris (27 out of 43, or 63%), and of those that do not, only 10 show a preference for a decreasing orbital period model (see Figure 2). Even fewer UHJs show any preference for a decreasing orbital period when we rescale ΔBIC to account for underestimated error (5 out of 43, or 12%), and the dropoff between ranked values is stark: while WASP-12 b boasts a rescaled ΔBIC > 300, the second-highest rescaled ΔBIC is for TrES-1 b, at 6.4, and the remaining three planets all fall below 2, indicating very marginal model preference. This lack of detection of period change for most systems presents an interesting question that we would like to take a first pass at answering: where *are* the decaying UHJs? Put another way: was WASP-12 b the first doomed world to be detected because it was one of the first to have enough transits and a long enough observational time span, or is there some feature of the WASP-12 system (e.g., its potential status as an evolved star) that sets it apart from most UHJ systems?

As noted in the Introduction, no fewer than 12 planets, not counting WASP-12 b and Kepler-1658 b, have had cases presented in the recent literature that performed similar

Table 7
Observational and Theoretical Constraints on Changing Period

	Derived from Observations							Theoretical Predictions		
Planet	$\dot{P}$ (ms yr^{-1})	σ	ΔBIC	ΔBIC Rescaled	Log $Q'_\star$	Log $Q_{\star,\min}$ [a]	τ (Myr)	Log $Q'_{\rm th}$	$\tau_{\rm th}$ (Myr)	$\lvert\dot{P}_{\rm th}\rvert$ (ms yr^{-1})
Systems with ΔBIC > 30										
WASP-12 b	-29.8 ± 1.6	18.5	947.1	337.1	1.6E+5	>5.1	3	10	6e+5	<0.01
WASP-46 b	22.6 ± 9.2	2.5	116.8	1.1	⋯	>4.8	⋯	6	5e+2	0.16
TrES-1 b	-16.4 ± 4.9	3.4	68.8	6.4	1.6E+2	>1.9	16	7	2e+5	<0.01
WASP-121 b	13.9 ± 3.3	4.2	37.6	13.0	⋯	⋯	⋯	10	2e+6	<0.01
Systems with ΔBIC < 30										
CoRoT-2 b	-2.4 ± 4.1	0.6	−1.8	−4.7	8.1E+4	>4.1	62	10	5e+6	<0.01
HAT-P-23 b [b]	-3.1 ± 2.5	1.3	−0.2	−3.2	3.2E+5	>5.0	33	7	8e+3	0.01
HAT-P-23 b [c]	-3.1 ± 2.5	1.3	−0.2	−3.2	3.2E+5	>5.0	33	10	1e+6	0.01
HAT-P-36 b	-6.1 ± 6.5	0.9	0.0	−4.0	1.3E+5	>4.5	19	6	3e+2	0.33
HATS-24 b	-4.5 ± 14.9	0.3	−3.8	−3.9	2.0E+5	>4.3	26	6	2e+2	0.42
HATS-35 b	-47.5 ± 43.8	1.1	0.4	−1.9	5.4E+3	>3.1	3	10	8e+6	<0.01
HATS-70 b	39.1 ± 68.6	0.6	−2.7	−2.7	⋯	>4.4	⋯	10	4e+5	<0.01
HIP 65 A b	22.3 ± 9.6	2.3	−2.1	0.7	⋯	>5.3	⋯	5.5	2e+1	2.62
KELT-16 b	-20.5 ± 12.5	1.6	1.8	−1.8	4.2E+5	>5.2	4	10	3e+5	<0.01
KELT-1 b	7.4 ± 7.8	0.9	1.6	−2.6	⋯	>6.3	⋯	10	6e+4	<0.01
KOI-13 b	-40.7 ± 136.8	0.3	−1.4	−2.0	5.2E+4	>3.7	4	10	6e+5	<0.01
KPS-1 b	93.7 ± 79.9	1.2	2.5	−2.6	⋯	>2.8	⋯	6	2e+3	0.06
Qatar-10 b	-52.4 ± 40.2	1.3	−1.9	−3.7	3.3E+3	>3.0	3	10	1e+7	<0.01
Qatar-1 b	-2.2 ± 2.9	0.8	−3.5	−5.0	6.6E+4	>4.1	56	6	6e+2	0.12
Qatar-2 b	-6.2 ± 6.6	0.9	2.7	−3.4	4.6E+4	>4.0	19	6	4e+2	0.21
TOI-2046 b	243.7 ± 107.6	2.3	0.4	0.5	⋯	>4.0	⋯	10	3e+6	<0.01
TOI-2109 b	5.8 ± 74.3	0.1	−4.5	−4.6	⋯	>5.7	⋯	8	2e+2	0.19
TOI-564 b	-86.0 ± 36.0	2.4	−2.6	1.7	3.1E+3	>3.1	2	6	8e+2	0.12
TrES-2 b	-5.9 ± 4.1	1.4	4.9	−3.4	3.1E+3	>3.0	36	6.5	8e+3	0.02
TrES-3 b	-4.0 ± 1.6	2.5	22.8	0.4	6.4E+4	>4.5	28	6	3e+2	0.27
WASP-18 b	-0.5 ± 1.1	0.5	−4.3	−4.5	3.6E+7	>6.7	156	10	5e+4	<0.01
WASP-19 b	0.6 ± 0.8	0.7	−4.4	−4.9	⋯	>6.4	⋯	5.5	2e+1	3.18
WASP-32 b	-48.7 ± 27.1	1.8	11.2	−0.1	1.2E+3	>2.7	5	6.5	2e+4	0.01
WASP-33 b	1.2 ± 4.7	0.2	−4.0	−4.6	⋯	>5.1	⋯	10	6e+5	<0.01
WASP-36 b	3.7 ± 3.9	0.9	−2.6	−3.6	⋯	>4.5	⋯	6	3e+2	0.28
WASP-3 b	-4.5 ± 5.1	0.9	−1.8	−4.2	7.4E+4	>4.2	36	10	3e+6	<0.01
WASP-43 b	-1.0 ± 1.1	0.9	−0.4	−4.6	1.7E+6	>5.6	70	5.5	3e+1	1.56
WASP-50 b	2.6 ± 12.8	0.2	−3.7	−3.9	⋯	>3.1	⋯	6.5	6e+3	0.02
WASP-52 b	-12.2 ± 6.4	1.9	19.3	−1.4	1.4E+3	>2.7	12	6.5	2e+4	0.01
WASP-5 b	-4.2 ± 4.0	1.1	−0.5	−3.2	6.9E+4	>4.3	34	6	8e+2	0.12
WASP-64 b	2.3 ± 6.5	0.4	−4.2	−4.3	⋯	>4.1	⋯	6	8e+2	0.12
WASP-77A b	4.1 ± 7.4	0.6	−3.4	−3.6	⋯	>4.3	⋯	6	4e+2	0.20
WASP-103 b	-4.1 ± 8.4	0.5	−3.2	−3.8	1.7E+6	>5.4	19	6	4e+1	1.29
WASP-104 b	5.0 ± 4.4	1.2	−2.7	−3.5	⋯	>4.0	⋯	6	1e+3	0.10
WASP-114 b	-28.4 ± 76.1	0.4	−1.2	−2.6	2.7E+4	>3.5	5	7	3e+3	0.03
WASP-135 b	-3.1 ± 8.0	0.4	−3.9	−3.8	1.1E+5	>4.1	39	6	3e+2	0.26
WASP-145A b	11.1 ± 10.8	1.0	−2.0	−2.0	⋯	>3.0	⋯	7	3e+4	<0.01
WASP-163 b	-8.2 ± 132.0	0.1	−2.7	−2.7	3.3E+4	>2.8	17	6	6e+2	0.15
WASP-164 b	-54.5 ± 25.1	2.2	13.6	1.2	2.5E+3	>3.0	3	6	8e+2	0.12
WASP-173A b	19.3 ± 11.0	1.8	1.1	−0.6	⋯	>5.0	⋯	6	1e+2	0.60

Notes.
[a] 3σ lower limit on $Q'_\star$ (in log base 10) as calculated from the lower limit on $\dot{P}$. No value if $\dot{P} - 3\sigma > 0$.
[b] HAT-P-23 theoretical calculations if using $M_\star = 0.58\ M_\odot$, $M_p = 1.34\ M_{\rm J}$, and $R_\star = 0.58\ R_\odot$.
[c] HAT-P-23 theoretical calculations if using $M_\star = 1.13\ M_\odot$, $M_p = 1.97\ M_{\rm J}$, and $R_\star = 1.19\ R_\odot$.

analyses and presented weak hints of period change. While not all of those planets have yet been included in our observing program, it is interesting to note that of the four that we have observed, we find instead a strong preference for a linear ephemeris for two (WASP-19 b using corrected data and WASP-43 b) and insignificant evidence for nonlinearity for the other two (TrES-2 b and TrES-3 b). Meanwhile, our single plausible candidate for a decreasing orbital period, TrES-1 b, is decreasing too quickly to be likely due to orbital decay (see Section 6.6).

Should we expect to have detected orbital decay in a substantial number of systems? To answer this question, we performed two simple tests to determine if we could have even detected decay as rapid as that of WASP-12 b. Theoretically,

Table 8
Could Have Detected WASP-12 b–Like Decay but Did Not

Planet	Observed ΔBIC	Test 1 Calc. ΔBIC if $\dot{P}$ like W12[a]	Observed $\dot{P}$	Test 2 Calc. $\dot{P}$ if $Q'_\star$ like W12[b]
WASP-12 b	947.1	896.1	-29.8 ± 1.6	-27 ± 1
WASP-43 b	−0.4	−7443.7	-1.0 ± 1.1	-10 ± 1.1
WASP-19 b	−4.4	−5861.1	0.4 ± 0.6[c]	-23 ± 0.8
WASP-18 b	−4.3	1597.9	-0.5 ± 1.1	-110 ± 1.1
TrES-3 b	22.8	1041.9	-4.0 ± 1.6	⋯
WASP-33 b	−4.0	335.0	1.2 ± 4.7[c]	⋯
HAT-P-23 b	−0.2	314.3	-3.2 ± 2.5	⋯
Qatar-1 b	−3.5	208.5	-2.2 ± 2.9	⋯
CoRoT-2 b	−1.8	180.4	-2.4 ± 4.1	⋯
WASP-121 b	37.6	129.8	14.0 ± 3.3[c]	⋯
Qatar-2 b	2.7	98.5	-6.2 ± 6.6	⋯
WASP-5 b	−0.5	77.9	-4.2 ± 4.0	⋯
HAT-P-36 b	0.0	70.2	-6.1 ± 6.5	⋯
KELT-1 b	1.6	60.8	7.4 ± 7.8[c]	-186 ± 7.8
WASP-103 b	−3.2	56.1	-4.1 ± 8.4	-40 ± 8.4
WASP-36 b	−2.6	55.6	3.7 ± 3.9[c]	⋯
WASP-52 b	19.3	49.5	-12.2 ± 6.4	⋯
TrES-2 b	4.9	44.1	-5.9 ± 4.1	⋯
WASP-3 b	−1.8	42.1	-4.5 ± 5.1	⋯
KELT-16 b	1.8	⋯	-20.5 ± 12.5	-50 ± 12.5
TOI-2109 b	−4.5	⋯	5.8 ± 74.3[c]	-641 ± 74.3

Notes.
[a] Test 1: analytical ΔBIC > 30 if WASP-12 b–like decay ($\dot{P} = -29$ ms yr^{-1}, Yee et al. 2020).
[b] Test 2: $\dot{P}$ significant by $\geqslant 3\sigma$ if $Q'_\star = 1.8 \times 10^5$ (Yee et al. 2020).
[c] Note: measured $\dot{P}$ is actually positive (increasing period).

we would expect a wide range of decay rates commensurate with the diverse stellar and planetary properties for these systems (see the range of predicted values in Table 7), but using WASP-12 b's relatively rapid rate sets a useful baseline against which to test our ability to detect tidal decay. The results of these tests are listed in Table 8. The first test assigns all planets the same rate of decay as WASP-12 b, $\dot{P} = -29$ ms yr^{-1} (Yee et al. 2020). We find that nearly half (18 out of 42 planets that are not WASP-12 b) would have had ΔBIC > 30, as shown in the Test 1 column in Table 8, while in reality only one did—and that planet, WASP-121 b, has a *positive* value for $\dot{P}$. Four systems (WASP-19 b, WASP-43 b, WASP-18 b, and TrES-3 b) would have ΔBIC values up to 10 times larger than that of WASP-12 b if they were decaying at the same rate, making the continued nondetection of decay in these systems highly significant.

We framed the second test to see what would have been observed if all stars had the same tidal dissipation factor. We assumed that every star had the same low value of $Q'_\star = 1.8 \times 10^5$ as WASP-12 b, also from Yee et al. (2020). We then calculated the rate of change $\dot{P}$ that would imply, and if the calculated value is equal to or greater than 3 times the observed error, then the planet is listed in Table 8. Seven planets, five of which also passed test 1, would have had 3σ results for $\dot{P}$ under test 2 (Table 8), including WASP-19 b, WASP-43 b, and WASP-18 b. Interestingly, the one planet for which we have the strongest claim for negative $\dot{P}$, TrES-1 b, did not pass this test: if it had a WASP-12 b–like $Q'_\star$, we would not have detected any change in period.

Thus, for 20 out of 42 systems, there is evidence that we could have detected WASP-12 b–like decay but have not, meaning these planets are likely to not be decaying as rapidly. The flip side of this statement is that for the other half of our sample (22/42 planets), we still do not have enough baseline to even detect decay as rapid as WASP-12 b. With the shortest of these planets having baselines that extend just 4 yr, it will take several more years to perhaps even decades to determine just how unusual WASP-12 b is.

7.2. Observational Constraints: Lower Limits on $Q'_\star$

In Table 7, we report values for $Q'_\star$ for systems with negative values of $\dot{P}$, even if they are statistically consistent with zero tidal decay. Recall that the value of $Q'_\star$ is inversely proportional to the rate of period change; the approximation used here is based on the formulation of Goldreich & Soter (1966):

$$Q'_\star = -\left(\frac{27\pi}{2}\right)\left(\frac{dP}{dt}\right)^{-1}\left(\frac{M_p}{M_s}\right)\left(\frac{a}{R_\star}\right)^{-5}. \quad (6)$$

For every system, we used the 3σ lower error to determine what the maximum decay rate is that would be consistent with the errors on $\dot{P}$, and if so, what the lower limit on $Q'_\star$ must be for it to not have been detected by our survey. For systems with a nominal negative value for $\dot{P}$, we also calculated an estimated decay lifetime, τ. For WASP-121 b, $\dot{P}$ is more than 3σ above 0, and we cannot place any constraint on $Q'_\star$, even a lower limit. For most of the systems, the constraints placed on $Q'_\star$ are much lower than any theory would predict, but we find that nine systems (9 out of 41, or 22%) must have $\log_{10} Q'_\star \geqslant 5.1$, the 3σ lower limit for WASP-12 (Table 7). Three systems (7%) can constrain $\log_{10} Q'_\star$ to be at least an order of magnitude larger than that of the star WASP-12: WASP-18 (6.7), WASP-19 (6.4), and KELT-1 (6.3). Again, it is important to note that we have neglected contributions to orbital decay from tidal

dissipation within the planets. Therefore, the constraints here on $Q'_\star$ are lower limits in this sense, too. Contributions from dissipation within the planets would allow $Q'_\star$ to be even larger than we report here and still be consistent with our observations.

7.3. Comparison to Theory

To place our observational constraints in a theoretical context, we used the grids from Weinberg et al. (2024) to estimate $Q'_\star$ for each system. We used Figures 5 and 7 from that paper and the best-fit system parameters from Table 3. Because the grid of calculated $Q'_\star$-values from that study is very coarse, instead of formally interpolating, we used a by-eye approximation. A major source of uncertainty is the large range in stellar age estimates, so we used the central value of the age estimate (when it exists). Note that HAT-P-23 shows up twice in Table 7 because of conflicting stellar mass estimates in the NASA Exoplanet Archive; we include both to illustrate how stellar uncertainty impacts these calculations.

The resulting theoretical estimates for $Q'_\star$ are listed as $Q'_{\rm th}$ in Table 3, and we computed the theoretical decay time $\tau_{\rm th}$ and rate of period decrease $\dot{P}_{\rm th}$ as in Equation (15) in Weinberg et al. (2024). For stellar models with radiative cores and convective envelopes, Weinberg et al. (2024) found values that range from $Q'_{\rm th} \approx \sim 10^5$ at $P = 0.5$ day to $Q'_{\rm th} \approx 10^6$–10^7 at $P = 2$ days. For higher-mass stars ($>1.2\ M_\odot$) on the main sequence, the cores are convective, and in such cases $Q'_\star$ is likely to be very large; for all such stars, we set $Q'_{\rm th} = 10^{10}$ as a representative value. If those stars were instead subgiants, however, as might be the case for WASP-12 b, their $Q'_\star$ would be much smaller, since their cores would become radiative.

Four systems are predicted, based solely on these theoretical estimates, to have rapid orbital decay as a result of having predicted $\log_{10} Q'_\star = 5.5$–6, with a theoretical prediction of $\dot{P}_{\rm th} < -1.0$ ms yr^{-1} for HIP 65 A b, WASP-103 b, WASP-19 b, and WASP-43 b (see Table 7). In two cases, WASP-19 b and WASP-43 b, the theoretical estimates (both have $\log_{10} Q'_{\rm th} = 5.5$) are actually lower than the current limits placed by our observations (respectively, $\log_{10} Q'_{\rm th} > 6.4$ and $\log_{10} Q'_{\rm th} > 5.6$), as can be seen in Figure 11. However, in both cases, the stellar age uncertainties are large: the age of WASP-19 is $5.5^{+8.5}_{-4.5}$ Gyr, while WASP-43's age is 7.0 ± 7.0 Gyr. If the stars were closer to the younger age, then we would predict correspondingly higher values for $\log_{10} Q'_\star$ and significantly slower decay rates (see panels on left side of Figure 5 in Weinberg et al. 2024).

8. Discussion and Conclusions

8.1. No Evidence Yet for Orbital Decay Being a Common UHJ Trait

Of the 43 planets with updated timing information presented in this work, just one—WASP-12 b—has clear indications of a period decrease that is likely due to orbital decay. In this work, we identify another system, TrES-1 b, which shows signs of a decreasing orbital period but at too rapid a rate to be due to orbital decay under any known theoretical prediction. We also have identified two systems, WASP-121 b and WASP-46 b, which show signs of increasing orbital period, though both systems have issues with existing data that may explain some or all of their purported period change.

For nearly half of our targets that are not WASP-12 b (20 out of 42), a case can be made that they are not experiencing orbital decay as rapidly as WASP-12 b or else we would have detected a 3σ value for $\dot{P}$, or $\Delta{\rm BIC} > 30$, or both. For a few systems (notably WASP-19 b, KELT-1 b, and WASP-18 b), the observations constrain orbital decay to be at least an order of magnitude slower, and $Q'_\star$ at least an order of magnitude greater, than that of the WASP-12 b system.

We note that of the two systems for which orbital decay is a credible explanation, both Kepler-1658 b (Vissapragada et al. 2022) and WASP-12 b (Weinberg et al. 2017) may have evolved off the main sequence, which could offer an explanation for more rapid decay (e.g., Weinberg et al. 2024). However, the status of the star WASP-12 is ambiguous (Leonardi et al. 2024), with a main-sequence star still favored (Bailey & Goodman 2019). If WASP-12 is in fact evolved, that would leave no main-sequence stars known to host decaying planets, offering support to predictions that orbital decay is unlikely during the main sequence and is a feature of later stages of stellar life. This is, however, in tension with the independent observation that hot Jupiter host stars are younger than all planet hosts (Hamer & Schlaufman 2019; Chen et al. 2023; Miyazaki & Masuda 2023) and that tidal decay does occur on the main sequence (Hamer & Schlaufman 2019). It is thus important to search more UHJs both on and off the main sequence for doomed worlds to see if this suggestive connection holds beyond a sample size of two planets.

We also note that for at least half of our sample, we lack sufficient data to have detected orbital decay even as rapid as that of WASP-12 b. It may be the case that identification of decaying planets around stars on the main sequence will require additional years of observations from either space (e.g., TESS) or ground-based observatories, in order for slower rates of orbital decay to reveal themselves. Based on calculations in this paper, we find that values for $Q'_\star$ probably span at least 3 orders of magnitude ($\sim 10^4$ for Kepler-1658 b, $\sim 10^5$ for WASP-12 b, and $>\sim 10^7$ for WASP-18 b). Predictions for the rates at which planets undergo orbital decay will have to take into account stellar mass and age.

8.2. Best Practices for Long-term Timing Analyses

We present three recommendations about best practices for timing analyses to search for orbital decay:

1. ΔBIC is a powerful tool for identifying systems of interest, especially accompanied by a significant value for $\dot{P}$. However, it is only as good as the error bars of the accompanying data. With the exception of a uniform data set for which the errors are well known (e.g., stacking all of the transits in a single Kepler quarter or TESS sector, as was done for Kepler-1658 b in Figure 10), it is likely that some errors are underestimated, increasing the apparent values for ΔBIC. Thus, when using ΔBIC with real data, it is important to understand that light curves in the published literature may have mistakes in both the absolute timing and the size of the nominal error bars. We recommend care in interpreting the ΔBIC results and suggest the tests described in this work, including the omit-one test to identify points that may be having an outsized impact on the apparent result and the rescaled ΔBIC test to identify if overall errors on the system may be too small. Given our experience in this work, ΔBIC

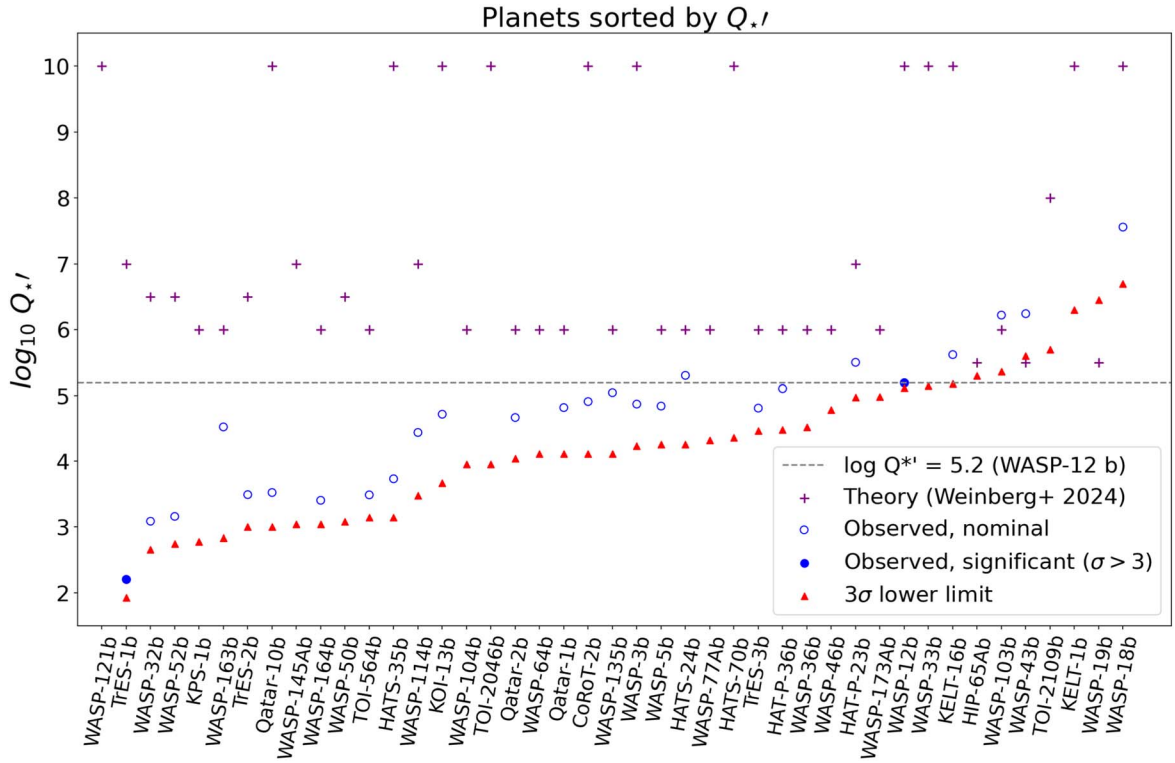

Figure 11. Constraints on $Q_\star'$ placed by observations. Lower limits are shown as upward-facing triangles and represent the 3σ lower limit for $Q_\star'$; these were calculated even for systems that had marginally positive values for $\dot{P}$ (increasing periods), so long as the 3σ value is below 0 (only WASP-121 b does not have this constraint). If $\dot{P}$ is nominally negative but insignificant ($<3\sigma$ detection), the corresponding value for $Q_\star'$ is shown as an open blue circle; the two systems with significant values for $\dot{P}$, WASP-12 b and TrES-1 b, are shown as filled blue circles. Finally, we plotted the theoretical estimates for $Q_\star'$ from Table 7 based on the work of Weinberg et al. (2024) as purple plus signs. See Table 7 for all parameter values.

values below 30–50 should be treated as tentative detections in need of confirmation.

2. In the ideal case, someone would observe a transit of every planet that might be experiencing orbital decay at least once a year to avoid long gaps in the timing data, following the recommendation of Jackson et al. (2023). We note for instance that WASP-121 b, which has very few distinct epochs available, would be a much clearer case if it had been more regularly observed in the years following its first announcement. Even relatively modest aperture telescopes, such as the 14 inch used in this work, are useful since many UHJs are found around sufficiently bright stars to constrain the transit timing. Widespread networks of small telescopes may also provide robust facilities for keeping ephemerides fresh and improving prospects for tidal decay detection (Peluso et al. 2023). In fact, phasing observations of a single transit conducted by multiple small telescopes simultaneously could result in a very high effective timing resolution, with the potential to significantly reduce midtransit time uncertainties.
3. There are timing errors in the literature, and the current system tends to propagate rather than eliminate errors. We identified errors spanning multiple published works in the timing of CoRoT-2 b and WASP-19 b. These errors had a strong effect, in that correcting them removed the signal of tidal decay entirely; but other errors may well be lurking that conform more to our expectations and thus have not been brought to light. We discuss this last item in detail in the next section.

8.3. The Timing Community Has a Database Problem

It is becoming clear that the scientific record is currently not well set up to facilitate long-term timing searches for slow changes over time involving multiple instruments and observers over many years. Timing errors, particularly conversion between times in UTC (what most data are recorded in) and BJD/TDB (what we need to use to detect true dynamical changes), are easy to make, hard to detect, and even harder to correct for posterity. Additionally, far too many early transit light curves have never been published except as figures in papers, removing valuable years of observational baseline from reanalysis. In some cases, not even a fitted midtime is available for individual light curves. And the current model of publication, whereby each new analysis publishes a list that combines midtimes of newly observed transits and times taken from the literature, has led to compilations of compilations of midtimes. We have documented multiple cases where this process has introduced errors in one work that are then propagated through later works.

The problem of data curation currently constitutes a major component of all long-term timing analyses. Rather than each group repeating the same effort to identify, extract, convert, reformat, and refit prior transit light-curve data, there should be a single archival database that contains a definitive list of all prior published transit times, as taken directly from their original publication. If more than one work has reported a time for a given transit, it should be clear which times are reanalyses, and a best time should be indicated, similar to how the NASA Exoplanet Archive reports all values for stellar

and planetary parameters but also provides a best value for researchers to use. This ideal transit timing database would provide information about each individual light curve and make transit light curves available for download in a uniform format to make it easy to refit data that are supposed to be in the public domain but in practice have been inconvenient to access. The ETD is an excellent resource and is well used by amateurs, but it is missing some key features (notably, it uses HJD/UTC instead of BJD/TDB timing and lacks a bulk download option for both light curves and the original JD times before conversion) and, moreover, has low uptake from the professional community. It would require either a substantial overhaul of the ETD or an entirely new system to be developed and funded for the long term.

In addition to observations of primary transits, an ideal timing database would also include timing constraints placed by planetary occultations (also called secondary eclipses). Occultations are even less likely to have published timing data available for individual light curves, owing to both their lower signal-to-noise and the propensity of occultation data to be used to study planetary atmospheres, where stacked and phased data of multiple occultations are necessary to tease out small signals. Occultation timing observations are used to determine if apsidal precession could explain a timing trend, since orbital decay will cause the interval between both transits and occultations to decrease, while precessing systems would have opposite trends, with occultations showing increasing periods while transits show decreasing periods, and vice versa.

Additionally, there should be an expectation shift that publishing data for a transit or occultation light curve requires publishing the photometric time series. Transit light curves can be archived as text files and do not require much data storage space compared to many astronomical data sets. Most journals can easily accommodate this data set as supplementary data files. Ideally, the published photometric light curves would also be required to be archived in a common format in the uniform transit timing database.

Finally, a thorough archival effort should be made to retrieve transit and occultation light curves that were used in prior works and may still exist on the hard drives of the original researchers, but which have not been made public, before the data are completely lost. These early transits and occultations provide critical data for constraining orbital decay. Without them, we will just have to wait longer to identify which worlds are doomed.

Acknowledgments

This study was supported by a grant from NASA's Exoplanet Research Program 21-XRP21-0170.

This paper uses observations made at the South African Astronomical Observatory (SAAO).

E.R.A. and A.A.S. were visiting astronomers at the Infrared Telescope Facility, which is operated by the University of Hawaii under contract 80HQTR19D0030 with the National Aeronautics and Space Administration. The authors wish to recognize and acknowledge the very significant cultural role and reverence that the summit of Maunakea has always had within the indigenous Hawaiian community. We are most fortunate to have the opportunity to conduct observations from this mountain, and we recognize that we are guests.

Data presented herein were obtained at the MINERVA-Australis facility from telescope time allocated under the NN-EXPLORE program with support from the National Aeronautics and Space Administration.

MINERVA-Australis is supported by Australian Research Council LIEF grant LE160100001, Discovery grants DP180100972 and DP220100365, the Mount Cuba Astronomical Foundation, and institutional partners the University of Southern Queensland, UNSW Sydney, MIT, Nanjing University, George Mason University, the University of Louisville, the University of California Riverside, the University of Florida, and the University of Texas at Austin.

We respectfully acknowledge the traditional custodians of all lands throughout Australia and recognize their continued cultural and spiritual connection to the land, waterways, cosmos, and community. We pay our deepest respects to all Elders, ancestors, and descendants of the Giabal, Jarowair, and Kambuwal nations, upon whose lands the MINERVA-Australis facility at Mt. Kent is situated.

ORCID iDs

Elisabeth R. Adams https://orcid.org/0000-0002-9131-5969
Brian Jackson https://orcid.org/0000-0002-9495-9700
Amanda A. Sickafoose https://orcid.org/0000-0002-9468-7477
Jeffrey P. Morgenthaler https://orcid.org/0000-0003-3716-3455
Hailey Stubbers https://orcid.org/0009-0005-2475-4987
Dallon Carlson https://orcid.org/0009-0001-5881-1856
Sakhee Bhure https://orcid.org/0000-0002-6673-8206
Chelsea X. Huang https://orcid.org/0000-0003-0918-7484
Nevin N. Weinberg https://orcid.org/0000-0001-9194-2084

References

Adams, E. R. 2010, PhD thesis, MIT
Adams, E. R., Jackson, B., Johnson, S., et al. 2021, PSJ, 2, 152
Adams, E. R., López-Morales, M., Elliot, J. L., Seager, S., & Osip, D. J. 2010, ApJ, 721, 1829
Adams, E. R., López-Morales, M., Elliot, J. L., Seager, S., & Osip, D. J. 2011, ApJ, 728, 125
Addison, B., Wright, D. J., Wittenmyer, R. A., et al. 2019, PASP, 131, 115003
Addison, B. C., Wright, D. J., Nicholson, B. A., et al. 2021, MNRAS, 502, 3704
Alonso, R., Auvergne, M., Baglin, A., et al. 2008, A&A, 482, L21
Alonso, R., Brown, T. M., Torres, G., et al. 2004, ApJL, 613, L153
Alsubai, K., Tsvetanov, Z. I., Pyrzas, S., et al. 2019, AJ, 157, 224
Anderson, D. R., Collier Cameron, A., Gillon, M., et al. 2012, MNRAS, 422, 1988
Anderson, D. R., Gillon, M., Maxted, P. F. L., et al. 2010, A&A, 513, L3
Astropy Collaboration, Price-Whelan, A. M., Lim, P. L., et al. 2022, ApJ, 935, 167
Astropy Collaboration, Robitaille, T. P., Tollerud, E. J., et al. 2013, A&A, 558, A33
Bailey, A., & Goodman, J. 2019, MNRAS, 482, 1872
Baluev, R. V., Sokov, E. N., Jones, H. R. A., et al. 2019, MNRAS, 490, 2246
Barker, A. J., Efroimsky, M., Makarov, V. V., & Veras, D. 2024, MNRAS, 527, 5131
Bayliss, D., Gillen, E., Eigmüller, P., et al. 2018, MNRAS, 475, 4467
Bouma, L. G., Winn, J. N., Howard, A. W., et al. 2020, ApJL, 893, L29
Bradley, L., Sipőcz, B., Robitaille, T., et al. 2019, astropy/photutils: v0.6, Zenodo, doi:10.5281/zenodo.2533376
Chen, D.-C., Xie, J.-W., Zhou, J.-L., et al. 2023, PNAS, 120, e2304179120
Chen, G., Pallé, E., Parviainen, H., et al. 2021, MNRAS, 500, 5420
Ciceri, S., Mancini, L., Southworth, J., et al. 2016, MNRAS, 456, 990
Collier Cameron, A., & Jardine, M. 2018, MNRAS, 476, 2542
Coppejans, R., Gulbis, A. A. S., Kotze, M. M., et al. 2013, PASP, 125, 976
Craig, M., Crawford, S., Seifert, M., et al. 2017, astropy/ccdproc: v1.3.0.post1, Zenodo, doi:10.5281/zenodo.1069648
Cortés-Zuleta, P., Rojo, P., Wang, S., et al. 2020, A&A, 636, A98
Davoudi, F., MirshafieKhozani, P., Paki, E., et al. 2021, AstL, 47, 638

Dawson, R. I., & Johnson, J. A. 2018, ARA&A, 56, 175
De, K., MacLeod, M., Karambelkar, V., et al. 2023, Natur, 617, 55
Delrez, L., Santerne, A., Almenara, J. M., et al. 2016, MNRAS, 458, 4025
Dragomir, D., Kane, S. R., & Pilyavsky, G. 2011, AJ, 142, 115
Eastman, J., Siverd, R., & Gaudi, B. S. 2010, PASP, 122, 935
Efroimsky, M., & Makarov, V. V. 2022, Univ, 8, 211
Espinoza, N., Rackham, B. V., Jordán, A., et al. 2019, MNRAS, 482, 2065
Foreman-Mackey, D., Hogg, D. W., Lang, D., & Goodman, J. 2013, PASP, 125, 306
Fox, C., & Wiegert, P. 2022, MNRAS, 516, 4684
Gillon, M., Lanotte, A. A., Barman, T., et al. 2010, A&A, 511, A3
Gillon, M., Triaud, A. H. M. J., Fortney, J. J., et al. 2012, A&A, 542, A4
Goldreich, P., & Soter, S. 1966, Icar, 5, 375
Guillot, T., & Havel, M. 2011, A&A, 527, A20
Guillot, T., & Showman, A. P. 2002, A&A, 385, 156
Gulbis, A. A. S., Bus, S. J., Elliot, J. L., et al. 2011, PASP, 123, 461
Hagey, S. R., Edwards, B., & Boley, A. C. 2022, AJ, 164, 220
Hamer, J. H., & Schlaufman, K. C. 2019, AJ, 158, 190
Harre, J. V., Smith, A. M. S., Barros, S. C. C., et al. 2023, A&A, 669, A124
Hebb, L., Collier-Cameron, A., Triaud, A. H. M. J., et al. 2010, ApJ, 708, 224
Hoyer, S., López-Morales, M., Rojo, P., Minniti, D., & Adams, E. R. 2016, MNRAS, 455, 1334
Hunter, J. D. 2007, CSE, 9, 90
Husnoo, N., Pont, F., Mazeh, T., et al. 2012, MNRAS, 422, 3151
Ivshina, E. S., & Winn, J. N. 2022, ApJS, 259, 62
Jackson, B., Adams, E. R., & Morgenthaler, J. P. 2023, AJ, 166, 142
Jackson, B., Greenberg, R., & Barnes, R. 2008, ApJ, 678, 1396
Johnson, J. A., Fischer, D. A., Marcy, G. W., et al. 2007, ApJ, 665, 785
Kanodia, S., & Wright, J. 2018, RNAAS, 2, 4
Kokori, A., Tsiaras, A., Edwards, B., et al. 2022, ExA, 53, 547
Lang, D., Hogg, D. W., Mierle, K., Blanton, M., & Roweis, S. 2010, AJ, 139, 1782
Liddle, A. R. 2007, MNRAS, 377, L74
Leonardo, P., Nascimbeni, V., Granata, V., et al. 2024, A&A, 686, A84
Maciejewski, G., Fernández, M., Aceituno, F., et al. 2021, A&A, 656, A88
Mannaday, V. K., Thakur, P., Southworth, J., et al. 2022, AJ, 164, 198
MAST Team 2021, TESS Light Curves—All Sectors, STScI/MAST, doi:10.17909/T9-NMC8-F686
Matsakos, T., & Königl, A. 2015, ApJL, 809, L20
Metzger, B. D., Giannios, D., & Spiegel, D. S. 2012, MNRAS, 425, 2778
Millholland, S., & Laughlin, G. 2018, ApJL, 869, L15
Miyazaki, S., & Masuda, K. 2023, AJ, 166, 209
Morello, G., Claret, A., Martin-Lagarde, M., et al. 2020a, JOSS, 5, 1834
Morello, G., Claret, A., Martin-Lagarde, M., et al. 2020b, AJ, 159, 75
Morgenthaler, J. P. 2022, jpmorgen/BigMultiPipe, v0.2.0, Zenodo, doi:10.5281/zenodo.7485043
Morgenthaler, J. P. 2023a, jpmorgen/ccdmultipipe, v0.0.2, Zenodo, doi:10.5281/zenodo.7507738
Morgenthaler, J. P. 2023b, Io Input/Output facility (IoIO) control, reduction, and analysis software, v1.1.1, Zenodo, doi:10.5281/zenodo.7703222
Morgenthaler, J. P., Rathbun, J. A., Schmidt, C. A., Baumgardner, J., & Schneider, N. M. 2019, ApJL, 871, L23
Moyano, M., Almeida, L. A., von Essen, C., Jablonski, F., & Pereira, M. G. 2017, MNRAS, 471, 650
Murgas, F., Pallé, E., Zapatero Osorio, M. R., et al. 2014, A&A, 563, A41
Nielsen, L. D., Bouchy, F., Turner, O., et al. 2019, A&A, 623, A100
Oliphant, T. E. 2006, A Guide to NumPy (USA: Trelgol Publishing), https://docs.scipy.org/doc/_static/numpybook.pdf
Osip, D. J., Phillips, M. M., Bernstein, R., et al. 2004, Proc. SPIE, 5492, 49
Öztürk, O., & Erdem, A. 2019, MNRAS, 486, 2290
Patra, K. C., Winn, J. N., Holman, M. J., et al. 2017, AJ, 154, 4
Patra, K. C., Winn, J. N., Holman, M. J., et al. 2020, AJ, 159, 150
Peluso, D. O., Esposito, T. M., Marchis, F., et al. 2023, PASP, 135, 015001
Penev, K., Bouma, L. G., Winn, J. N., & Hartman, J. D. 2018, AJ, 155, 165
Penev, K., Jackson, B., Spada, F., & Thom, N. 2012, ApJ, 751, 96
Petrucci, R., Jofré, E., Ferrero, L. V., et al. 2018, MNRAS, 473, 5126
Petrucci, R., Jofré, E., Gómez Maqueo Chew, Y., et al. 2020, MNRAS, 491, 1243
Poddaný, S., Brát, L., & Pejcha, O. 2010, NewA, 15, 297
Pu, B., & Lai, D. 2019, MNRAS, 488, 3568
Rauer, H., Erikson, A., Kabath, P., et al. 2010, AJ, 139, 53
Rosário, N. M., Barros, S. C. C., Demangeon, O. D. S., & Santos, N. C. 2022, A&A, 668, A114
Schwarz, G. 1978, AnSta, 6, 461
Sedaghati, E., Boffin, H. M. J., MacDonald, R. J., et al. 2017, Natur, 549, 238
Sun, L., Gu, S., Wang, X., et al. 2023, MNRAS, 520, 1642
Sun, Z., Ji, J.-h., & Dong, Y. 2018, ChA&A, 42, 101
Tregloan-Reed, J., Southworth, J., & Tappert, C. 2013, MNRAS, 428, 3671
Tsiaras, A., Waldmann, I. P., Rocchetto, M., et al. 2016, ApJ, 832, 202
Virtanen, P., Gommers, R., Oliphant, T. E., et al. 2020, NatMe, 17, 261
Vissapragada, S., Chontos, A., Greklek-McKeon, M., et al. 2022, ApJL, 941, L31
Wang, W., Zhang, Z., Chen, Z., et al. 2023, ApJS, 270, 14
Wang, X.-Y., Wang, Y.-H., Wang, S., et al. 2021, ApJS, 255, 15
Weinberg, N. N., Davachi, N., Essick, R., et al. 2024, ApJ, 960, 50
Weinberg, N. N., Sun, M., Arras, P., & Essick, R. 2017, ApJL, 849, L11
Wittenmyer, R. A., Clark, J. T., Trifonov, T., et al. 2022, AJ, 163, 82
Yang, F., & Wei, X. 2022, PASP, 134, 024401
Yee, S. W., Winn, J. N., Knutson, H. A., et al. 2020, ApJL, 888, L5
Yeh, L.-C., Jiang, I.-G., & A-thano, N. 2024, NewA, 106, 102130
Zhou, G., Bakos, G. Á, Bayliss, D., et al. 2019, AJ, 157, 31